Macromolecules

pubs.acs.org/Macromolecules Article

Surface Charge Density and Steric Repulsion in Polyelectrolyte–Surfactant Coacervation

Jason J. Madinya, Hansen Tjo, Xiangxi Meng, Isaac A. Ramírez Marrero, Charles E. Sing,* and Sarah L. Perry*

Cite This: *Macromolecules* 2023, 56, 3973–3988 Read Online

ACCESS | Metrics & More | Article Recommendations | Supporting Information

ABSTRACT: Solutions of oppositely charged polyelectrolytes and surfactants can undergo phase separation, in a charge-driven process known as complex coacervation. These materials are widely used in a variety of applications because of their useful rheological and structural properties. It is understood that these properties are related to the assembly of the surfactants into micelles, which then undergo complexation with the oppositely charged polyelectrolytes to form the coacervate phase. However, there remain challenges in understanding how the molecular features of the components give rise to this useful phase behavior, with a still-nascent understanding of how electrostatics, micelle structure, composition, and steric interactions interplay to govern coacervation. In this paper, we used a combination of experiment and a recently developed hybrid simulation/theory model to understand polyelectrolyte–surfactant coacervates. We used mixtures of ionic and neutral surfactants to systematically vary the micelle surface charge density, along with PEG side-chains on the neutral surfactants to vary the steric repulsions between nearby micelles. Finally, we altered the polyelectrolyte charge density to tune the polymer-mediated attractions between micelles. By mapping the phase behavior of these solutions, we showed that higher charge density on the polymer or micelle, or decreasing steric repulsion, facilitates coacervation. We considered analogous quantities in our simulation/theory model, which makes predictions for both the thermodynamics and the structure of the micelle–polyelectrolyte rich coacervate and micelle–polyelectrolyte poor supernatant phases. By varying the micelle surface charge density and the correlation-based polymer–micelle interaction energy, we showed phase separation behaviors consistent with experiments.

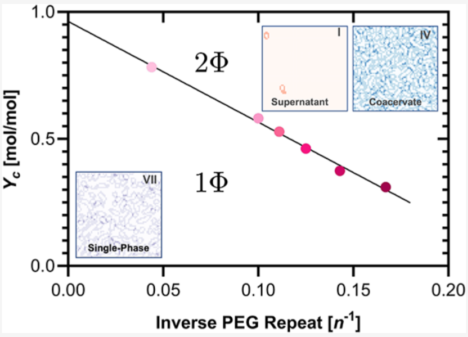

■ INTRODUCTION

Complexes of oppositely charged polyelectrolytes and surfactants can undergo a charge-driven, liquid–liquid phase separation known as complex coacervation.[1−8] Coacervation in this situation is driven by the electrostatic attractions between the oppositely charged macromolecules, resulting in a macromolecule-dense liquid phase known as the coacervate phase and a macromolecule-dilute phase known as the supernatant. The phase behavior of these coacervates (e.g., the stability of the coacervate against dissolution by salt) depends on a variety of molecular parameters including polyelectrolyte charge density,[7,9−11] surfactant micelle surface density,[3,7,11] polyelectrolyte molecular weight,[3,7,12−14] solution ionic strength,[2,7,11] solution pH,[15] and surfactant architecture.[6,7,12] Variations in the phase behavior can also be used to describe changes in the rheological properties of the material[16−23] and can affect the partitioning or solubility of both coacervate-forming and guest components.[24−27]

Complex coacervates have a long history of use in applications ranging from food additives[28−30] to personal care products[31−35] and pharmaceutical products.[36−38] An important feature of polyelectrolyte–surfactant coacervates that makes them useful in so many applications is the way in which their phase behavior is governed by the assembly of the surfactant species. The identity and combinations of these surfactants can be tailored to control the interactions relevant to coacervation. In particular, multivalent interactions are facilitated by the self-assembly of the surfactants into micellar structures; this either occurs when the surfactant concentration is above its critical micelle concentration (CMC) or, in the presence of oppositely charged polyelectrolytes, the critical aggregate concentration (CAC). The CAC is typically lower than the CMC of the surfactant alone because the oppositely charged polyelectrolyte facilitates the formation of micelles by neutralizing the electrostatic repulsion between charged surfactant heads.[7,39−42] Above the CAC, the surfactants will undergo coassembly with the polyelectrolytes into micellar structures to form supramicellar aggregates[5,11,13−15,41,43−45]

Received: March 13, 2023
Revised: May 3, 2023
Published: May 30, 2023

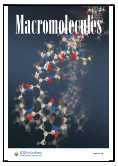

https://doi.org/10.1021/acs.macromol.3c00464
Macromolecules 2023, 56, 3973−3988

such as spherical vesicles and cylindrical micelle structures.[5,41,46−49]

Experimentally, the phase behavior of polyelectrolyte−surfactant mixtures has been studied across a range of different systems.[2,7,8,11,13,14,23,45,50−55] The majority of these reports have leveraged mixed micelles containing a combination of ionic and nonionic surfactants[2,7,8,11,13,14,23,55−59] as the strength of the electrostatic interactions between a pure ionic micelle and a polyelectrolyte can lead to solid precipitation rather than liquid coacervation. The introduction of nonionic surfactants leads to the formation of mixed micelles, where the surface charge of the micelle is controlled by the proportion of charged to uncharged surfactants in solution. In particular, many reports leverage titration experiments to determine the minimum ionic content necessary within a micelle to drive complexation, a parameter termed Y_c.[1−4,55−60] In addition to modulating the surface charge density of the micelle, the nonionic surfactants can also impact the interactions between the surfactant micelles and the polyelectrolyte in other ways. For instance, the presence of a bulky, water-soluble headgroup can create a steric barrier against complexation and alter the geometry of the micelle.[60−65] The chemical identity of the headgroup can also affect the solubility of the complex through solvent interactions.[55]

In addition to considering the effects of the surfactant species, studies have also examined the ways in which the physicochemical properties of the polyelectrolytes can affect complexation. In particular, we were inspired by work by Dubin and co-workers, who have reported on the effect of molecular features on complexation in a variety of systems.[11,55] In one more recent study, experiments to compare Y_c in a system of the anionic surfactant sodium dodecyl sulfate (SDS) and the neutral surfactant TX-100 with either poly(diallyldimethylammonium chloride) (PDADMAC) or poly(trimethylaminoethyl methacrylate) (PTMAEMA) as the cationic polyelectrolyte were performed.[55] The authors attributed the lower value of Y_c observed for the PTMAEMA system to the higher charge density of the polymer compared with PDADMAC (i.e., PTMAEMA has a roughly 3 spacing between charges compared to 6 for PDADMAC). Thus, the higher charge density of the polymer allowed for a decrease in the charge density of the micelle. A similar result was observed for the system of dimethyldodecylamine oxide (DMDAO) in the presence of either poly(2-acrylamido-2-methylpropanesulfonic acid, sodium salt) (PAMPS) or a lower charge density copolymer with *N*-vinylpyrrolidone (P(AMPS-NVP)).[11]

The study by Fan et al. also looked to examine the impact of the neutral surfactant.[55] In particular, they compared complexation between systems containing TX-100 as the neutral surfactant with a $C_{13}E_{11}$ Brij surfactant.[55] Brij surfactants consist of a linear alkyl tail (in this case 13 carbons long), coupled to a water-soluble poly(ethylene glycol) (PEG) headgroup (chain length 11).[55] In contrast, TX-100 has a complex aromatic/branched alkyl hydrophobic tail coupled with a 10-monomer-long PEG chain. Regardless of the choice of polyelectrolyte, surfactant micelles containing the $C_{13}E_{11}$ showed a higher Y_c value, meaning that a higher micellar charge density was required for the system to undergo coacervation, than did micelles containing TX-100.[55] This result hints at potential steric effects created by the neutral surfactant headgroup, as the longer PEG chain present on $C_{13}E_{11}$ would potentially impose a larger separation distance between the approaching polyelectrolyte and the sulfate groups buried at the polar/nonpolar interface of the micelle, thereby decreasing the strength of the electrostatic interactions. However, for this specific study it is difficult to deconvolute the effects of the headgroup from those of the two different hydrophobic tails and how they might affect surfactant packing within a micelle.

Overall, reports from the literature suggest that the ability for surfactant−polyelectrolyte systems to undergo complex coacervation at a given set of solution conditions is a function of the combined charge density of the polyelectrolyte and the surfactant micelles and that this interaction can be further modulated by steric effects.[55,59−61,63−66] There is an opportunity to further elucidate these effects and help to develop a more general understanding of the physics underlying these types of self-assembling systems through tailored experiments with model surfactants and polymers.

Theory and simulation can provide complementary insight into how the molecular features of the surfactant and polymer species affect coacervate phase behavior. Despite the breadth of experimental study into surfactant−polyelectrolyte coacervation, modeling has only been used occasionally to predict how molecular features affect phase behavior.[67] One common approach is to modify Flory−Huggins theory to reflect the measured phase behavior of model surfactant−polyelectrolyte coacervates.[6,68] However, this neglects both electrostatic and structural features, relying on parametrization of these systems that is not predictive or physically interpretable in the context of molecular interactions. Several efforts alternatively invoke an abstract one-dimensional binding representation, known as the Satake−Yang model, to accompany isothermal titration calorimetry data.[5,42,48,51,69,70] This approach is similar to developments in polyelectrolyte−polyelectrolyte coacervates[71−75] but is also essentially empirical and neglects the rich three-dimensional structure inherent to surfactant−polyelectrolyte coacervates. Molecular simulation has also been used to model complexation between surfactant micelles and polyelectrolytes.[47,76−80] This approach has the advantage that it can directly capture molecular structure and electrostatics but is unable to reach the length and time scales relevant for predicting phase behavior and coacervation. These computational approaches are only able to account for a few individual micelles, rather than an entire micelle-based phase.[47,76−78,81] Finally, there has been theoretical progress in understanding complexation and coacervation in related polyelectrolyte−nanoparticle or polyelectrolyte−protein solutions. The Ganesan group used a combination of polymer field theory and single-chain in mean-field simulations to understand the distribution of polyelectrolytes around uniform and patchy particles and relate to phase behavior.[82−86] Recently, Rumyantsev et al. also developed scaling arguments for polyelectrolyte−particle coacervates.[87] Both of these approaches predict coacervation due to the fluctuation-driven attraction between charged colloids that are “bridged” by an oppositely charged polyelectrolyte chain with low linear charge density.

Recently, the authors have developed a new hybrid simulation and field theory model to predict surfactant−polyelectrolyte coacervation.[88] This model uses self-consistent field theory (SCFT) to model the polyelectrolytes in solution, which interact with the surfactant micelle surface through external potential fields generated using Monte Carlo (MC) simulations. This model builds on ion-pairing concepts that were developed in previous work modeling polyelectrolyte−

polyelectrolyte coacervation,[71−75,89,90] where the high-charge-density environment of the coacervate phase and high linear charge density of the polyelectrolyte allowed us to model the charge−charge interactions through ion pairing. Importantly, however, this model directly accounts for both the electrostatic interactions at the molecular level and the structural asymmetry inherent in complexation between flexible polymers and the oppositely charged surfactant micelle.

In this paper, we seek to use both systematic experimental study and molecular modeling to understand surfactant−polyelectrolyte coacervation, studying how phase separation is affected by modulating the interactions between a standard polycation and anionic mixed surfactant micelles. We show that there is a trade-off between increasing the micelle surface charge density, controlled by the composition of a mixture of neutral and anionic surfactants, and the steric repulsion between nearby micelles, controlled by short, grafted PEG chains on the neutral surfactants. Corresponding quantities are identified in hybrid simulation/theory models, providing a physical and molecular interpretation of this trade-off that is consistent with experiments. Experiments also demonstrate that polyelectrolyte linear charge density has a similar effect on surfactant−polyelectrolyte coacervation. Qualitative agreement between experiments and modeling provides the foundation for studying how molecular interactions affect phase behavior in polyelectrolyte−surfactant mixtures.

■ EXPERIMENTAL METHODS

Materials. All reactants, 2-(dimethylamino)ethyl methacrylate (DMAEMA, 98%, Sigma-Aldrich), iodomethane (99%, Sigma-Aldrich), 2-hydroxyethyl methacrylate (HEMA, 98%, Sigma-Aldrich), 4-cyano-4-(phenylcarbonothioylthio)pentanoic acid (Sigma-Aldrich), 4,4-azobis(4-cyanovaleric acid) (ACVA, Sigma-Aldrich), and dioxane (anhydrous, 99.8%, Sigma-Aldrich) were used as received.

The anionic surfactant sodium dodecyl sulfate (SDS) and the neutral Brij surfactants polyoxyethylene(6)lauryl ether (L_6), polyoxyethylene(8)lauryl ether (L_8), and polyoxyethylene(9)lauryl ether (L_9) were purchased from Sigma-Aldrich. Polyoxyethylene(7)-lauryl ether (L_7) (>99%) was purchased from Anatrace. Polyoxyethylene(10)lauryl ether (L_{10}) and polyoxyethylene(23)lauryl ether (L_{23}) were purchased from Fisher Scientific. Sodium chloride (NaCl) was also purchased from Fisher Scientific. The cationic homopolymer poly([2-(methacryloyloxy)ethyl] trimethylammonium chloride) (PTMAEMA) was a gift from BASF. Deionized (DI) water was obtained from a Milli-Q water purification system (resistivity of 18.2 MΩ cm, Millipore).

Cationic Monomer Synthesis. Cationic monomers for the polymers were prepared by the quaternization of commercially available DMAEMA (Figure S1a). DMAEMA (15 g, 95.4 mmol) was first dissolved in THF (150 mL, dry) in a flask submerged in an ice bath, followed by degassing with nitrogen for 1 h. An excess of iodomethane (27.1 g, 190.1 mmol) was then added dropwise into the solution. The resulting mixture was stirred under nitrogen gas for 1.5 h in the ice bath and then allowed to react further at room temperature for 24 h. The product, [2-(methacryloyloxy)ethyl] trimethylammonium iodide (TMAEMA), precipitated out of solution and was filtered and rinsed with diethyl ether before drying under vacuum overnight. The successful quaternization reaction reached 99% conversion of DMAEMA, determined by proton nuclear magnetic resonance spectroscopy (^{1}H NMR, Bruker Avance III 500 MHz spectrometer) using 5 mm diameter tubes in deuterated water (D_2O, 98%, Acros Organics) at 25 °C (Figure S1b).

Copolymer Synthesis and Characterization. All copolymers used in this work were synthesized by reversible addition−fragmentation chain transfer (RAFT) polymerization (Figure S2). RAFT was chosen because of the ability to precisely control the molecular weight of polymers from monomers of various chemical functionalities in different reaction conditions.[91−93] The total targeted degree of polymerization (N) was ∼100 for all copolymers. Copolymers with varying charge content were synthesized by controlling the feed molar ratio between TMAEMA and HEMA. Synthesis was performed using a TMAEMA:HEMA ratio of 25:75, 50:50, and 75:25. 4-Cyano-4-(phenylcarbonothioylthio)pentanoic acid was used as a chain transfer agent (CTA), and ACVA was used as the initiator in all reactions at a molar ratio of 10:1 (CTA:initiator). Each copolymer was synthesized at a total polymer scale of 5 g. All reactants were fully dissolved in 20 mL of dioxane in a 50 mL round-bottom flask and degassed with nitrogen for 1 h with constant stirring. The flask was then placed in an oil bath at 70 °C for 14 h. The polymerization was quenched by immersing the flask into an ice bath. The copolymer was precipitated and purified by adding the product solution dropwise into acetone. The solid copolymer product was redissolved in water and precipitated in acetone. This purification was repeated three times. The resultant polymer product, poly([2-(methacryloyloxy)ethyl] trimethylammonium iodide)-*r*-2-hydroxyethyl methacrylate (PTMAEMA-*r*-HEMA, Figure 1), was then lyophilized (Labconco FreeZone 2.5 Plus) and stored in a −20 °C freezer until further use. The number-averaged molecular weight (M_n) and the average degree of polymerization (N) for the PTMAEMA-*r*-HEMA copolymers were determined based on end-group analysis from ^{1}H NMR spectroscopy in D_2O (Figure S3 and Table S1).

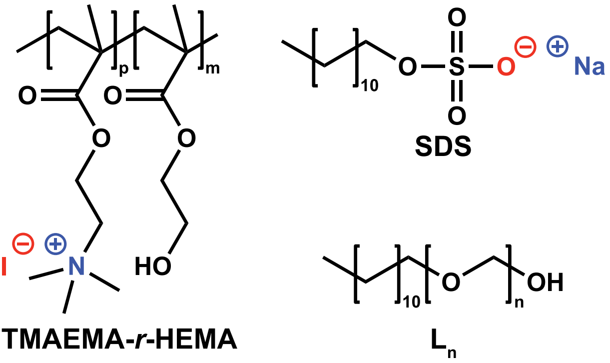

Figure 1. Chemical structures of the cationic polymer PTMAEMA-*r*-HEMA, anionic surfactant SDS, and nonionic Brij surfactants (L_n, where L refers to the dodecyl lauryl alkyl tail and n refers to the length of the PEG chain) used in this investigation.

Diffusion Ordered Spectroscopy (DOSY) Characterization of the PTMAEMA Homopolymer. The weight-averaged molecular weight (M_w) of the PTMAEMA homopolymer was determined using ^{1}H diffusion ordered spectroscopy (DOSY) NMR. A 0.5% w/w polymer solution in 250 mM KBr (99%, Alfa Aesar) in D_2O was prepared and pipetted into a 3 mm NMR tube (Norrell C-S-3-400-7). The NMR used was a Bruker Avance III 400 MHz spectrometer. All experiments were performed without spinning. The 90° pulse (p) was calibrated before each measurement. Bipolar sine-squared shaped gradients were used with a total duration of $2{\cdot}p30$ where $p30$ was typically 1 ms. Gradient recovery delays were 0.10.5 μs. The number of gradient steps was set to be 16. Individual rows of the quasi-2D diffusion databases were phase corrected and baseline subtracted. The DOSY data were then processed using MestReNova 14.0 by examining the decay of the area under the curve of a peak, where the diffusion coefficient was determined based on a three-parameter exponential function to describe the decay. The peak used for this analysis was the triple methyl group around the quaternary amine for PTMAEMA (Figure S4). The hydrodynamic radius (R_h) was calculated using the Stokes−Einstein equation $R_h = \frac{kT}{6\pi\eta_s D}$, where k is the Boltzmann constant, T is the temperature in kelvin, η_s = 0.89 mPa/s is the viscosity of water, and D is the diffusion coefficient determined via DOSY in m^2/s. A relationship between molecular

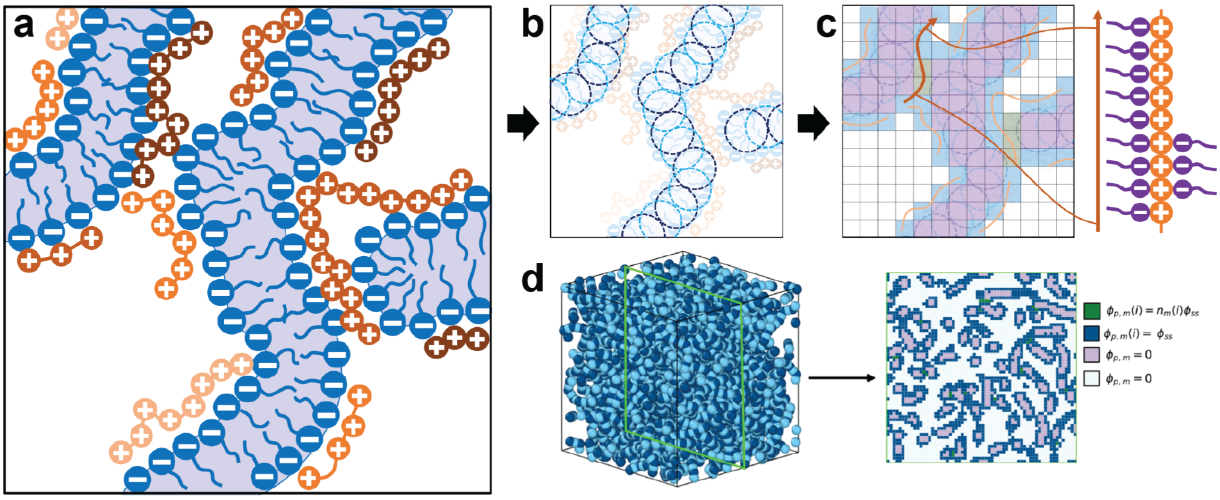

Figure 2. Schematic illustrating our hybrid theory/simulation scheme. (a) This paper focuses on electroneutral mixtures of surfactants and oppositely charged polycations in solution, characterized by a volume fraction $\langle \phi_{pm} \rangle$. These systems are modeled first by (b) representing wormlike micelle structures as touching beads with interstitial beads used to more closely reflect the cylindrical structure. MC simulations of this model are run, and then snapshots (c) are mapped to a "grid" of sites, where the surface sites (blue, green) form a polycation-binding field and the micelle interior sites (purple) exclude polycation monomers. SCFT calculations enumerate the polymer conformations (orange lines), where each monomer along the chain is affected by the fields that account for singly paired (blue, $n_{m,i} = 1$) and double-paired (green, $n_{m,i} = 2$) situations (schematic on the right). (d) Representative simulation snapshot (left) and a corresponding grid representation from a 2-D slice (right).

weight (g/mol) and the R_h (nm) based on poly(methyl methacrylate) was used to convert R_h to the molecular weight of the PTMAEMA homopolymer studied, $M_w = 2030 R_h^{1.908}$. This relationship was obtained by determining the diffusion coefficient of various poly(methyl methacrylate) samples of different molecular weights (from 2.2 to 287 kg/mol) in deuterated chloroform using the same procedure previously described and relating the diffusion coefficient with the molecular weight determined by an absolute MW-determination method (as supplied by the manufacturer). Salt was added to suppress the charge interactions and allow for PTMAEMA to behave more like a neutral polymer in a good solvent. Using this method, we obtained a diffusion coefficient of $D = 3.57 \times 10^{-11}$ m^2/s and $M_w = 80$ kg/mol, corresponding to a degree of polymerization $N = 385$.

Stock Solution Preparation. Surfactant stock solutions were prepared gravimetrically at a concentration of 20 mM. Polycation stock solutions were prepared gravimetrically at a concentration of 10 mM on an ionizable monomer basis. Stock solutions of NaCl were prepared gravimetrically at a concentration of 2 M. All solutions were prepared using Milli-Q water.

Coacervate Sample Preparation. Polyelectrolyte−micelle coacervate samples were prepared in 1.5 mL microcentrifuge tubes (Fisherbrand). Milli-Q water, NaCl solution, polycation, nonionic surfactant, and then anionic surfactant were added in such order at room temperature (25 °C). Samples were vortexed for 10 s following the addition of all reagents to ensure complete mixing. The total sample volume was 500 L, which enhanced mixing and reduced bubble formation due to the high surface activity of the surfactants. All samples were prepared at a final salt concentration of 625 mM NaCl with a 1:1 molar ratio of polycation (on an ionizable monomer basis) to anionic surfactant unless otherwise specified.

Micellar Charge Fraction. The phase behavior of the various coacervate systems was determined to be a function of the composition of the mixed micelles, and we defined a fractional composition of anionic surfactant Y. This quantity is assumed to be proportional to the average micellar surface charge density[11,55] and is defined as

$$Y = \frac{[\text{anionic surfactant}]}{[\text{anionic surfactant}] + [\text{neutral surfactant}]} \tag{1}$$

In experiments, we changed this quantity Y independently while maintaining charge stoichiometry between the micelle and polyelectrolyte components; the concentrations of polycation and anionic surfactant were held constant, and we varied the concentration of the nonionic surfactant component. We were able to determine the critical micellar surface charge density Y_c above which coacervation occurs. For a given polyelectrolyte−micelle system, 15 different samples spanning a range of micellar charge fractions were prepared and analyzed by turbidity and optical microscopy. Data points were selected to aid in determining the critical micellar surface charge density Y_c for each system. This meant that for polyelectrolyte−micelle systems with polycation species of lower charge densities, or nonionic surfactants with longer PEG repeats, samples to determine the critical micellar surface charge density were concentrated at a higher value of Y than for systems with higher charge density polymers or shorter PEG chain surfactants.

Turbidity. Immediately following preparation, 60 L of each of the coacervate samples was pipetted, in triplicate, into a clear flat bottom 384-well plate (Fisher Scientific) for turbidity and microscopy analysis. Turbidity was recorded at a wavelength of $\lambda = 562$ nm using a microplate reader (Bio Tek Synergy H1) after 10 s of orbital shaking. The turbidity (τ) was defined as $\tau = -\ln(I/I_0)$, where I represents the intensity of light that passed through the sample volume and I_0 represents the incident light intensity. All measurements were performed in triplicate and subtracted from a reference sample of Milli-Q water. Error bars on turbidity plots indicate the standard deviation of replicate measurements. Measurements were performed in triplicate with a 10 min delay between reads and were subtracted from a reference sample of Milli-Q water.

Optical Microscopy. Following turbidimetry, optical microscopy was used to confirm the presence of phase separation in each sample. Optical micrographs were obtained for each sample using an EVOS XL Core optical microscope (Fisher Scientific) with a 40× objective. Imaging was performed within 30 min of incubation at room temperature (25 °C) following sample preparation.

■ COMPUTATIONAL METHODS

We modeled the phase behavior of surfactant−polyelectrolyte coacervates through a hybrid Monte Carlo−self-consistent field theory (MC-SCFT) model developed in our previous work,[88] and we refer to that paper for a detailed description of our scheme and its predictions. Here, we give a brief accounting of this model and how we map it to the

https://doi.org/10.1021/acs.macromol.3c00464
Macromolecules 2023, 56, 3973−3988

experimental system. In our simulation/theory hybrid model, the surfactant micelle structure was determined from MC simulations, using a bead−rod representation with bending potentials to account for its wormlike structure. We assume a wormlike micellar structure due to experimental evidence for this morphology in the literature at the relatively high surfactant concentrations associated with coacervation.[94−96] Snapshots of these simulations were mapped to a grid and used to construct external potential fields in our SCFT model that account for the location and interactions associated with the surface and interior sites within the micelle geometry. The SCFT calculation, performed over several micelle configurations, was then used to obtain a system free energy. While we will discuss each aspect of this scheme below, Figure 2 illustrates the overall workflow of this calculation, which uses the two different methods to account for the disparate time and length scales associated with the micelle versus polymer species.

In this theoretical model, we considered a limited parameter space suggested by Svensson et al. to simplify how the five-component polyelectrolyte−surfactant coacervates are represented.[54,97] They used a portion of parameter space that removes one of the components, and in our case we took that to be the counterion of the surfactant. The remaining species were then combined into electroneutral components that can fully describe the system composition in terms of volume fraction: the water solvent ϕ_W, a polymer−salt component ϕ_{ps}, and a polymer−micelle component ϕ_{pm}. This allowed us to express coacervation in a quasi-2D phase diagram (see ref 88). Here, we have simplified the parameter space further and only considered electroneutral mixtures of polymer and micelle (i.e., $\phi_{ps} \to 0$, Figure 2a). This was not rigorously true in the experimental system, which included counterions for both the polymer and micelle species, as well as added salt, but we will take this limit as a useful proxy for the ability to undergo coacervation. We justify this choice by noting that by not including any of the salt species, the theoretical phase boundaries represent the limit of maximum phase separation for a given polyelectrolyte−surfactant pair.[88]

Monte Carlo Simulation of Micelle Structure. Micelle configurations were generated using MC simulations, which represent cylindrical wormlike micelles as bonded hard-sphere chains. Our minimalist model used the potential $\tilde{U}_m$:

$$\tilde{U}_m = \tilde{U}_{hs} + \tilde{U}_b + \tilde{U}_\theta = \sum_i \sum_{j>i} \tilde{u}_{hss,ij} + \sum_i{}' \tilde{u}_{b,i,i+1} + \sum_i{}' \tilde{u}_{\theta,i,i+1,i+2} \tag{2}$$

This potential included pairwise hard-sphere and bond potentials ($\tilde{U}_{hs}$ and $\tilde{U}_b$, respectively) and a bond angle potential $\tilde{U}_\theta$ between three consecutive bonded beads (see Figure 2b). Each of these contributions is the sum over individual pairwise or three-body contributions, $\tilde{u}_{hs,ij}$, $\tilde{u}_{b,i,i+1}$, and $\tilde{u}_{\theta,i,i+1,i+2}$, with the apostrophes on the summations indicating that only indices between bonded beads were included in the sum and tildes denoting normalization of energies by k_BT. For the hard-sphere potential, each pairwise contribution $\beta u_{hs,ij}$ is given by

$$\tilde{u}_{hs,ij} = \begin{cases} 0 & r_{ij} \geq \sigma_{hs} \\ \infty & r_{ij} < \sigma_{hs} \end{cases} \tag{3}$$

Here, r_{ij} is the distance between beads i and j and σ_{hs} is the hard-sphere diameter of the beads. The pairwise bonding potentials $\tilde{u}_{b,i,i+1}$ are given as

$$\tilde{u}_{b,i,i+1} = \begin{cases} 0 & r_{i,i+1} \leq 1.01\sigma_{hs} \\ \infty & r_{i,i+1} > 1.01\sigma_{hs} \end{cases} \tag{4}$$

Finally, the three-body bending potentials $\tilde{u}_{\theta,i,i+1,i+2}$ are given as

$$\tilde{u}_{\theta,i,i+1,i+2} = \frac{\tilde{\kappa}_\theta}{2}\theta^2_{i,i+1,i+2} \tag{5}$$

To parametrize this model, we simply considered a value of the bending constant $\tilde{\kappa}_\theta = 3.3$ that was used in our previous work[88] and yielded a persistence length consistent with typical micelle geometries given in the literature.[98] We also do not include an explicit micelle−micelle attraction in this model, which would be needed for complete consistency with the SCFT predictions;[88] this simplification is primarily rationalized by the high concentration of the coacervate phase which does not leave much room for perturbations to the micelle structure due to attractions.

MC simulations were performed using a standard Metropolis criterion, using translational moves with an acceptance probability given by $p_{acc} = \min[1, \exp(-\Delta\tilde{U}_m)]$, where $\Delta\tilde{U}_m$ is the change in the potential for a given move. The MC simulations were performed at hard-sphere volume fractions ϕ_{hs} ranging from $\phi_{hs} = 0.01$ to $\phi_{hs} = 0.50$, and five samples were run for each concentration. The box length was set at $L = 17\sigma_{hs}$, and the simulations were run for 100×10^6 MC steps, with translational moves for all monomers attempted once per MC step.

We used one snapshot from each of the five independent simulation trajectories to generate the external potential fields used in the SCFT portion of the calculations. Noninteracting spheres were then added halfway between the bonded hard spheres to approximate the cylindrical geometry (Figure 2b). The simulation box was then gridded into $M^3 = 64^3$ collocation points, and sites were designated as micelle interior, surface, or exterior sites (Figure 2c). This grid size was chosen to balance computational efficiency and resolution and does not affect our predictions beyond modest discretization effects. Surface sites were further characterized by the number of nonconsecutive micelle segments $n_{m,i}$ overlapping with the boundaries of the collocation points. The set of grid points were then used to create two spatially varying fields, $\tilde{\varepsilon}_m(\mathbf{r})$ and $\tilde{\Omega}(\mathbf{r})$, where the former accounts for the surfactant−polymer interactions at the micelle surface and the latter accounts for the exclusion of the polymer from the micelle interior. We defined $\tilde{\varepsilon}_m(\mathbf{r})$ both spatially and with respect to the number of surface sites:

$$\tilde{\varepsilon}_m(\mathbf{r}) = \begin{cases} \tilde{\varepsilon}^0_m & \text{surface sites, } n_{m,i} = 1 \\ \tilde{\varepsilon}^0_m + \tilde{\varepsilon}^1_m & \text{surface sites, } n_{m,i} > 1 \\ 0 & \text{all other sites} \end{cases} \tag{6}$$

We parametrized this potential by distinguishing surface sites adjacent to a single micelle as interacting with an adsorption energy $\tilde{\varepsilon}^0_m$ and surface sites adjacent to multiple micelles as having an *additional* interaction energy $\tilde{\varepsilon}^1_m$. Both of these parameters represent electrostatic interactions in this system, which is accounted for via ion pairing interactions that have a magnitude set by the Coulomb interactions between particles at contact (related to the dimensionless Bjerrum length) rather than an explicit inclusion of the $1/r$ Coulomb potential. This is an established approach to account for charge correlation effects such as counterion condensation,[99,100] recently demonstrated to be a dominant driving force for polyelectrolyte–polyelectrolyte coacervation.[101] We expect an analogous condensation effect on the surface of the surfactant micelles.[102,103] The $\tilde{\varepsilon}_{\mathrm{m}}^{1}$ contribution accounts for the charge-driven correlations between micelle surfaces, which is an energetic benefit of having two immediately adjacent micelles. These correlations are well established in the literature[104,105] and manifest as like-charged attractions between highly charged surfaces with oppositely charged polyelectrolyte chains in between.[106−108] In this work, we account for this phenomenon as emerging from the extra electrostatic attraction ($\tilde{\varepsilon}_{\mathrm{m}}^{1}$) that a charged monomer has with two nearby surfaces rather than just a single surface ($\tilde{\varepsilon}_{\mathrm{m}}^{0}$). We note that this notation is slightly different from our previous work, which simply assumed that $\tilde{\varepsilon}_{\mathrm{m}}^{0} = \tilde{\varepsilon}_{\mathrm{m}}^{1}$. We made this change of notation to independently change the two contributions because we will attribute changes in $\tilde{\varepsilon}_{\mathrm{m}}^{1}$ to steric effects due to grafted PEG chains. The field $\tilde{\Omega}(\mathbf{r})$ also varies spatially:

$$\tilde{\Omega}(\mathbf{r}) = \begin{cases} 10 & \text{interior sites} \\ 0 & \text{all other sites} \end{cases} \tag{7}$$

The choice of $\tilde{\Omega} = 10$ is arbitrary but large and was intended to almost completely exclude polymers from the micelle interior. Finally, we also used the MC simulations to determine the density field for the number of possible micelle-bound polyelectrolyte segments $\rho_{\mathrm{m}}(\mathbf{r}) = \phi_{\mathrm{ss}} n_{\mathrm{m},i}/\nu_{\mathrm{p}}$, which is related to the local volume fraction of surface sites ϕ_{ss} and a monomer reference volume ν_{p}. This will be related to the experimental variable Y, which is the fraction of charged surfactants in the mixed-surfactant system, where we relate the surface site volume fraction to a fully charged $\phi_{\mathrm{ss},0}$, via $\phi_{\mathrm{ss}} = Y\phi_{\mathrm{ss},0}$. In our model, Y thus relates to the number of surfactant–polymer interactions. We obtained this combination of the fields $\rho_{\mathrm{m}}(\mathbf{r})$, $\tilde{\Omega}(\mathbf{r})$, and $\tilde{\varepsilon}_{\mathrm{m}}(\mathbf{r})$ for five snapshots at a given volume fraction of the micelle–polymer component ϕ_{pm}, and these grids were used in the SCFT portion of the calculation (see examples in Figure 2d).

SCFT Model. The fields determined from the MC part of our model are incorporated into a SCFT model to account for the entire set of chain conformations and how they are affected by nonbonded interactions in the system. This calculation yields a partition function that contributed to the free energy of the coacervate, specifically accounting for the conformations and interactions of the polyelectrolyte species.

For this standard SCFT calculation, the polyelectrolytes are modeled as Gaussian chains, where the bonded potential is expressed as[109]

$$\tilde{U}_{\mathrm{b}}[\mathbf{r}] = \frac{3}{2b^2} \sum_{i}^{n_{\mathrm{p}}} \int_0^{N_{\mathrm{s}}} \mathrm{d}s_i \left| \frac{\mathrm{d}\mathbf{r}_i(s_i)}{\mathrm{d}s_i} \right|^2 \tag{8}$$

Here, b is the segment length, N_{s} is the number of segments in a chain, n_{p} is the number of chains, and s is the segment index along the chain. Besides being a standard assumption in SCFT calculations,[110] the use of a Gaussian chain model is consistent with experimental evidence that polyelectrolytes in dense coacervate phases exhibit Gaussian chain statistics.[16,111] All the segments along the chain are assumed to be paired with either the surfactant micelle surface or an oppositely charged salt ion (Figure 2c). The interactions along the chain with the salt and surfactant micelle are captured through the binding potential for each segment, which we developed in our prior work[88] and depends on its bound state; $\Psi_{\mathrm{s}} = M$ for micelle-bound segments, and $\Psi_{\mathrm{s}} = S$ for salt-bound segments. The polyelectrolyte chain is treated as a series of adsorption sites, with a nonbonded potential U_{nb} for the overall chain given in our previous work as[88]

$$\tilde{U}_{\mathrm{nb}} = \sum_{i}^{n_{\mathrm{p}}} \int_0^{N_{\mathrm{s}}} \mathrm{d}s_i [\tilde{\varepsilon}_m(\mathbf{r}(s_i))\delta(\Psi_{s_i} = M) + \tilde{\varepsilon}_s \delta(\Psi_{s_i} = S) + \boldsymbol{\Omega}(\mathbf{r}(s_i))] \tag{9}$$

The potential fields $\tilde{\varepsilon}_{\mathrm{m}}(\mathbf{r}(s_i))$ and $\tilde{\boldsymbol{\Omega}}(\mathbf{r}(s_i))$ are determined from the MC portion of the calculation. The parameter $\tilde{\varepsilon}_{\mathrm{s}}$ corresponds to the binding energy between the polyelectrolyte and salt, which we do not use in this paper because we assume the limit $\phi_{\mathrm{ps}} \to 0$. The configurational partition function for the polyelectrolyte can be expressed as

$$\mathcal{Z}_{\mathrm{c}} = \frac{z_0^{n_{\mathrm{p}}}}{n_{\mathrm{p}}!} \prod_{i}^{n_{\mathrm{p}}} \sum_{\{\Psi_{s_i}\}} \int \mathcal{D}\mathbf{r}_i \exp(-\beta(U_{\mathrm{b}}[\mathbf{r}^{n_{\mathrm{p}}N_{\mathrm{s}}}] + U_{\mathrm{nb}}[\mathbf{r}^{n_{\mathrm{p}}N_{\mathrm{s}}}])) \tag{10}$$

To solve this partition function, the particle to field transformation was performed as described in the monograph by Fredrickson.[109] The resulting field-based partition function is expressed as

$$\mathcal{Z}_{\mathrm{c}} = \frac{z_0^{n_{\mathrm{p}}}}{n_{\mathrm{p}}!} \int \mathcal{D}\rho_{\mathrm{m}} \int \mathcal{D}\omega_{\mathrm{c}} \prod_{i}^{n_{\mathrm{p}}} \int \mathcal{D}\mathbf{r}_i \sum_{\Psi_i} \exp\left(-\beta U_{\mathrm{b}} + i \int \mathrm{d}\mathbf{r}\, \omega_{\mathrm{c}}(\rho_{\mathrm{m}} - \hat{\rho}_{\mathrm{p,m}})\right) \exp\left(-\sum_{i}^{n_{\mathrm{p}}} \int_0^{N_{\mathrm{s}}} \mathrm{d}s_i [\tilde{\varepsilon}_{\mathrm{m}}(\mathbf{r}(s_i)) + \boldsymbol{\Omega}(\mathbf{r}(s_i))]\right) \tag{11}$$

where ω_{c} is an auxiliary constraining field that is conjugate to the density field. The operator $\hat{\rho}_{\mathrm{p,m}}(\mathbf{r})$ is the operator that reports the micelle-bound polymer segment density at position $\mathbf{r}$, which we want to constrain to the micelle binding site density field ρ_{m}. The operator is defined as

$$\hat{\rho}_{\mathrm{p,m}}(\mathbf{r}) = \sum_{i}^{n_{\mathrm{p}}} \int \mathrm{d}s_i\, \delta(\mathbf{r} - \mathbf{r}(s_i))\delta(\Psi_{s_i} = M) \tag{12}$$

The field-based partition function was solved numerically using the pseudospectral method described by Fredrickson.[109] We refer the reader to our previous publication[88] for the details regarding the particle to field transformation as well as the numerical solution scheme for the SCFT. This scheme finds the value of ω_{c}^{*} that extremizes the Hamiltonian:

$$\mathcal{H}[\rho_{\mathrm{m}}, \omega_{\mathrm{c}}] = -i \int \mathrm{d}\mathbf{r}\, \omega_{\mathrm{c}}(\mathbf{r})\rho_{\mathrm{m}}(\mathbf{r}) - n_{\mathrm{p}} \ln Q[i\omega_{\mathrm{c}}] \tag{13}$$

This yields a value for the single-chain partition function $Q[i\omega_{\mathrm{c}}^{*}]$that is a functional of ω_{c}^{*}, defined as $Q[i\omega_{\mathrm{c}}^{*}] = V^{-1}\sum_{\Psi_N}\int \mathrm{d}\mathbf{r}\, q(\mathbf{r}, s = N, \Psi_N; [i\omega_{\mathrm{c}}])$, where $q(\mathbf{r}, s = N, \Psi_N; [i\omega_{\mathrm{c}}])$ is the single-chain propagator that describes the Boltzmann factor for a chain ending at a location $\mathbf{r}$ and in a pairing state Ψ_N. We again refer back to our previous paper for details on how to calculate this quantity.[88] This scheme can be used to calculate the spatially varying volume fractions $\phi_{\mathrm{p},M}$ and $\phi_{\mathrm{p},S}$ that are the volume fractions of polymer chains in state M and S, respectively, though in the case of the $\phi_{\mathrm{ps}} \to 0$ limit considered here we merely calculated $\phi_{\mathrm{p}}(\mathbf{r}) = \phi_{\mathrm{p},M}(\mathbf{r}) = -n_{\mathrm{p}}\, \delta$

$\ln Q[i\omega_c^*]/\delta(i\omega_c(\mathbf{r}))$. This is related to the overall composition variable via the relationship $\phi_{pm} = 2\langle\phi_{p,M}\rangle + \phi_{hc}$, which includes both the surface site and bound polymer volume fraction in the first term as well as the hard-core volume fraction from the MC calculation. With these quantities, we can numerically calculate the free energy from SCFT, F_{SCFT}:

$$\frac{\nu_p\beta F_{SCFT}}{V} = \frac{\nu_p\beta}{V}F_0 + \frac{\phi_p}{N_p}\ln\phi_p - i\frac{1}{M^3}\sum_j^{M^3}\omega_{c,j}\phi_{p,j} - \frac{\phi_p}{N_p}\ln Q[i\omega_c^*] \tag{14}$$

F_0 is an arbitrary reference free energy that includes contributions that are either zero- or first-order in concentration and thus thermodynamically unimportant. The subscript j denotes the values of, e.g., $\phi_p(\mathbf{r})$ at the discrete collocation point $\mathbf{r}_j$, such that $\phi_{p,j}$ corresponds to the polymer segment density at collocation point j. The overall SCFT free energy contribution (F_{SCFT}) corresponds to the contribution of the polyelectrolyte to the solution free energy. The other contribution relevant to this paper is the excluded volume of the surfactant micelles F_{cs} which is approximated using the Carnahan–Starling equation of state:[112]

$$\frac{\nu_p\beta F_{cs}}{V}(\phi_m{}') = \frac{\nu_m}{\nu_p}\frac{\phi_m{}'}{\nu_m}\frac{4\phi_m{}' - 3\phi_m{}'^2}{(1-\phi_m{}')^2} \tag{15}$$

where ν_m is the volume of the micelle hard-sphere particle from the MC simulations and ϕ'_m is the volume fraction of the micelle chain including the noninteracting interstitial particles and the hard-sphere chain particles from the MC simulations. We could in principle determine a more accurate form for this contribution from simulation, but for practicality assume that the Carnahan–Starling expression for hard-sphere liquids is reasonably close to our coacervate model which represents the micelles by a high density of connected spherical particles. The expression for the solution free energy can now be expressed as a function of the polymer–micelle complex concentration ϕ_{pm}:

$$\begin{aligned}\frac{\nu_p\beta F}{V} &= \frac{\nu_p\beta}{V}(F_{SCFT} + F_{cs}) = \frac{\nu_p\beta}{V}F_0 + \frac{\phi_p}{N_p}\ln\phi_p - i\frac{1}{M^3}\sum_j^{M^3}\omega_{c,j}\phi_{p,j} \\ &\quad - \frac{\phi_p}{N_p}\ln Q[i\omega_c] + \frac{\nu_m}{\nu_p}\frac{\phi'_m}{\nu_m}\frac{4\phi'_m - 3\phi'^{\,2}_m}{(1-\phi'_m)^2}\end{aligned} \tag{16}$$

This free energy will allow us to track phase behavior as a function of the surface site density ϕ_{ss} and the micelle–micelle correlation energy $\tilde{\varepsilon}^1_m$, whose connection to the experimental parameters will be discussed in the Results section.

RESULTS AND DISCUSSION

The goal of this study was to understand how factors like charge density and steric hindrance from factors like grafted PEG chains modulate the ability for polyelectrolyte–surfactant complex coacervates to undergo phase separation. To this end, we leveraged experiments using well-defined polyelectrolytes and surfactants in combination with MC-SCFT simulation approaches to characterize a model system and elucidate the molecular physics governing electrostatic versus steric interactions. Qualitative agreement between both approaches allows us to connect surfactant design with parameters in theoretical predictions, opening up the possibility for fundamental understanding of these otherwise complicated phenomena.

Experimental Characterization of Polyelectrolyte–Surfactant Coacervate Formation. The majority of reports describing coacervation between a polyelectrolyte and an oppositely charged surfactant micelle have leveraged mixed micelles containing a combination of ionic and nonionic surfactants to modulate the strength of the electrostatic interaction and allow for liquid–liquid phase separation rather than solid precipitation.[2,5,7,8,11,23,27,55−58] Here, we looked to understand how the ability of a system to undergo complex coacervation is altered by (i) modulating the micelle surface charge density through the inclusion of nonionic surfactants to weaken electrostatic interactions, (ii) tuning the steric hindrance between the charges on the micelle and the complexing polyelectrolyte, and (iii) comparing the effect of tuning surfactant properties with the effect of changing the charge density of the polymer.

To explore the effect of micelle charge density, we used a mixture of the anionic surfactant sodium dodecyl sulfate (SDS) with various nonionic Brij surfactants (Figure 1). To minimize the potential for structural variations arising from packing within the hydrophobic core of the micelle, all of the Brij surfactants used in this study had a dodecyl tail so as to match that of SDS. We also examined Brij surfactants with different length PEG headgroups (n = 6, 7, 8, 9, 10, 23) to test the effect of a steric barrier on complexation. As dodecyl-based surfactants are often termed *lauryl*, we will use the nomenclature L_n to refer to these various surfactants. Lastly, we explored the effect of polymer charge density through the use of random copolymers of PTMAEMA-*r*-HEMA (Figure 1).

To determine the conditions where polyelectrolyte–surfactant micelle solutions phase separate, we exploited the increase in turbidity that arises from droplet formation. Using both turbidimetry and optical microscopy experiments, we determined a critical anionic surfactant mole fraction $Y = Y_c$ at which phase separation began to occur. The quantity Y is a monotonic and titratable parameter with which the phase behavior of polyelectrolyte–micelle systems can be tuned independently of ionic strength, as well as polyelectrolyte and micellar chemistries, and has been widely used in the literature.[1−4,55−60]

We show in Figure 3 a typical turbidimetric titration experiment with PTMAEMA-SDS/L_6 as the polyelectrolyte–micelle system, performed at a constant 1:1 charge stoichiometry. Here, we drove phase separation by titrating the anionic surfactant SDS, thereby incrementally increasing Y such that the solution eventually becomes cloudy. We identified the critical micellar surface charge density Y_c as the point at which a sharp increase was observed in turbidity, corresponding with the onset of phase separation. In Figure 3, for the case of PTMAEMA-SDS/L_6 we observed this steep change in solution turbidity to have taken place at Y = 0.32. We also verified the onset of phase separation via optical microscopy. Moreover, we observed that turbidity values further increased with Y for $Y > Y_c$, which we attributed to an increase in the electrostatic interactions that favor phase separation, though we did not explore the limit of this effect.

We used this approach to experimentally investigate the phase behavior of a variety of polyelectrolyte–micelle systems to examine how the critical micellar surface charge density for coacervation can be modulated by molecular properties. To understand the relationship between electrostatic attraction and steric repulsion in polyelectrolyte–micelle coacervation,

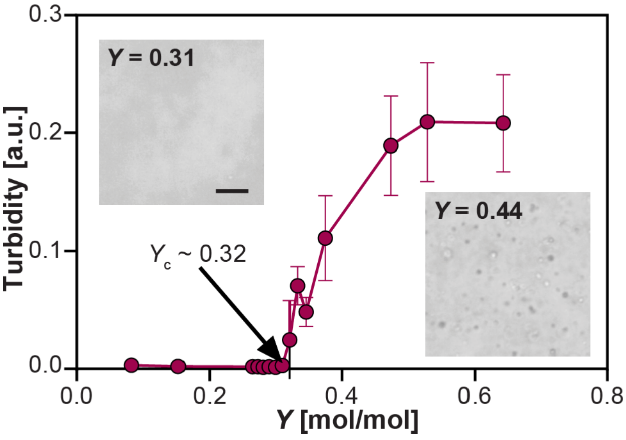

Figure 3. Turbidity as a function of Y for the system of PTMAEMA-SDS/L_6 at a constant 1:1 charge stoichiometry and 625 mM NaCl. Optical micrographs indicate the absence or presence of phase separation at the specified value of Y. Scale bar is 25 μm.

we performed turbidimetric titration experiments for a panel of Brij-L_n nonionic surfactants with different lengths of the PEG repeat units (n = 6, 7, 8, 9, 10, 23). We hypothesized that the number of repeat units n would change the effective distance of approach between surfactant micelles, independent of the charge density of both the polyelectrolyte and surfactant micelle. As shown in Figure 4, the results of both the turbidimetric titration and optical microscopy show that the critical fraction of anionic surfactants Y_c increases with the length of the PEG repeats present in the neutral surfactant. Upon increasing the PEG chain from n = 6 to n = 23, the fraction of anionic surfactants needed to drive phase separation more than doubled from Y_c = 0.32 to Y_c = 0.75. These results support our hypothesis, suggesting that stronger electrostatic interactions (i.e., a higher micellar charge density) are needed to overcome increased steric repulsion from the longer PEG chains. In addition, although we did not quantify the extent of phase separation (such as the volume or distribution of coacervates), visual inspection of the samples via optical microscopy suggested that qualitatively, the system containing L_{23} resulted in a significantly lower number of coacervate droplets compared to other L_n systems (Figure 4b). We speculate that the relatively high steric forces in L_{23} compared to the shorter PEG chain surfactants may suppress the electrostatic correlations that drive phase separation.

We also sought to examine the importance of the molecular properties of the polyelectrolyte in modulating phase behavior. In particular, we compared the phase behavior of coacervates formed from different random PTMAEMA-*r*-HEMA copolymers of varying charge density. Interestingly, we were only able to observe phase separation for polyelectrolyte charge densities of 100% and 75%; no phase separation was observed for polyelectrolyte charge densities of 50% and 25% for any of the surfactant systems tested in this study. Furthermore, at a polyelectrolyte charge density of 75% we were only able to observe phase separation with the least sterically hindered surfactants L_6 and L_7; subsequent mixed micelles with longer PEG chains did not demonstrate phase separation at any of the conditions tested.

Figure 5a shows the critical surface charge density Y_c for the two different charge density polyelectrolytes and the neutral surfactants L_6 and L_7. Our results demonstrate that decreasing the polyelectrolyte charge density significantly increased the minimum micellar surface charge density Y_c needed for phase separation. The strong dependence of coacervate formation on linear charge density is consistent with the literature on polyelectrolyte−polyelectrolyte coacervates due to the importance of local charge correlations on the electrostatic attractions that drive phase separation.[24,89,90,113]

Polyelectrolyte−Surfactant Micelle Coacervation from Hybrid Simulation/Field Theory Model. Experimentally, we demonstrated how the surfactant micelle composition and steric repulsion due to PEG chains compete to govern coacervation phase behavior. Using molecular models, we can show that by relating these quantities to the micelle surface charge density and local correlation-based interactions between micelles, we can make phase diagram predictions consistent with experiments. Our hybrid simulation/theory scheme specifically identifies two parameters as related to their experimental counterparts: (i) the anionic surfactant surface site volume fraction per micelle ϕ_{ss} is proportional to the anionic surfactant mole fraction Y, and (ii) the magnitude of the micelle−micelle charge correlation energy $\tilde{\varepsilon}_{\mathrm{m}}^{1}$ is inversely related to the length of the grafted PEG chains, n, for the L_n surfactants.

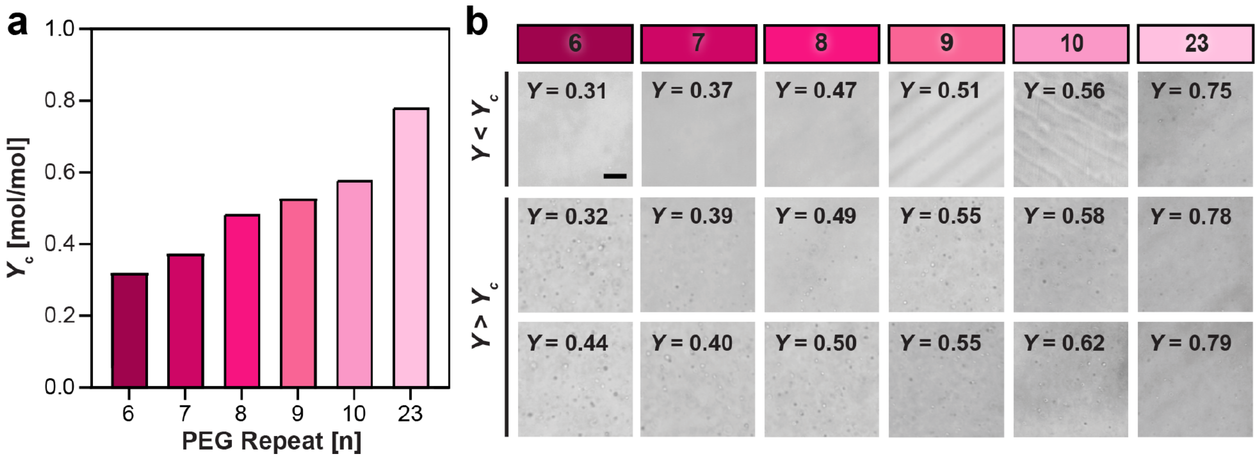

Figure 4. (a) Plot of Y_c as a function of PEG length n illustrating the effects of increasing steric exclusion on critical micelle surface charge density. (b) Corresponding optical micrographs that span a range of Y values above and below Y_c. Scale bar is 25 μm.

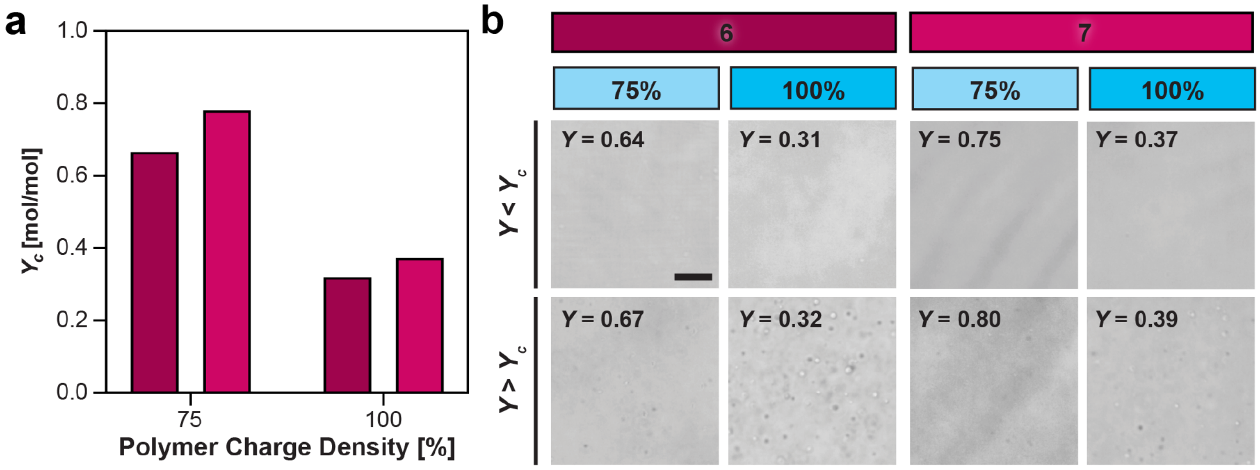

Figure 5. (a) Plot of Y_c vs polymer charge density as a relative fraction of charged TMAEMA to neutral HEMA groups, illustrating the effects of cationic polymer charge density on the critical micellar surface charge densities of mixed micelles with distinct PEG lengths (n = 6, 7). (b) Corresponding optical micrographs over a range of Y values both above and below Y_c. Scale bar is 25 μm.

We first solved the SCFT model to obtain the system free energy F as a function of the polymer−micelle complex concentration ϕ_{pm}, the main compositional variable in our model, as a function of the tunable parameters $\tilde{\varepsilon}_m^1$ and ϕ_{ss}. The solution behavior of the system can be determined by constructing the free energy manifold and using the common tangent construction to find regions of coexistence. We again note that in this paper we consider the limit that $\phi_{ps} \to 0$ as this represents the region of maximum phase separation; in our previous work,[88] it was determined that increasing the solution ionic strength by increasing the polymer−salt complex concentration decreased the propensity for a solution to undergo coacervation. We also consider that the surfactants self-assemble into disordered wormlike micelles, a simplifying assumption given the large variety of structures that can be formed in polyelectrolyte−surfactant systems.[5,41,46−49] In principle, this assumption can be relaxed, but we expect that the relationship between molecular interactions and the coacervate thermodynamics will only quantitatively be affected by the assembled surfactant structure. We will consider these structural effects in future work.

Figure 6 shows the system free energy $\nu_p \beta F/V$ as a function of ϕ_{pm} for several different parameters $\tilde{\varepsilon}_m^1$ and ϕ_{ss}. Figure 6a plots several values of the micelle−micelle interaction energy $\tilde{\varepsilon}_m^1$ at a constant $\phi_{ss} = 0.04$. Figure 6b conversely plots several values of the surface charge density ϕ_{ss} at a fixed value of $\tilde{\varepsilon}_m^1 = -3.50$. For visualization purposes, a thermodynamically irrelevant linear term $a \times \phi_{pm}$ was added to the free energies, where a was chosen to allow the free energy at the coexisting common tangent points to be approximately equal, and the plots were shifted so the free energy at the common tangent points of all the plots are equal. This allows for visual comparison between the different free energy curves corresponding to changes in $\tilde{\varepsilon}_m^1$ and ϕ_{ss}.

In Figure 6a, the coacervate phase polymer−micelle complex concentration ϕ_{pm}^c is given by the rightmost series of common tangent points, denoted by open circles. Conversely, the supernatant phase concentration ϕ_{pm}^s is given by the leftmost series of common tangent points. The distance between the two concentrations $\phi_{pm}^c - \phi_{pm}^s$ increased with increasing values of the magnitude of $|\tilde{\varepsilon}_m^1|$, which we interpret as an increase in the excess polyelectrolyte-mediated correlation energy between nearby micelle surfaces. In our previous work,[88] this enhancement to the micelle−polyelectrolyte binding energy was shown to be necessary for phase separation to occur and is thus the driving force for coacervation in polyelectrolyte−surfactant

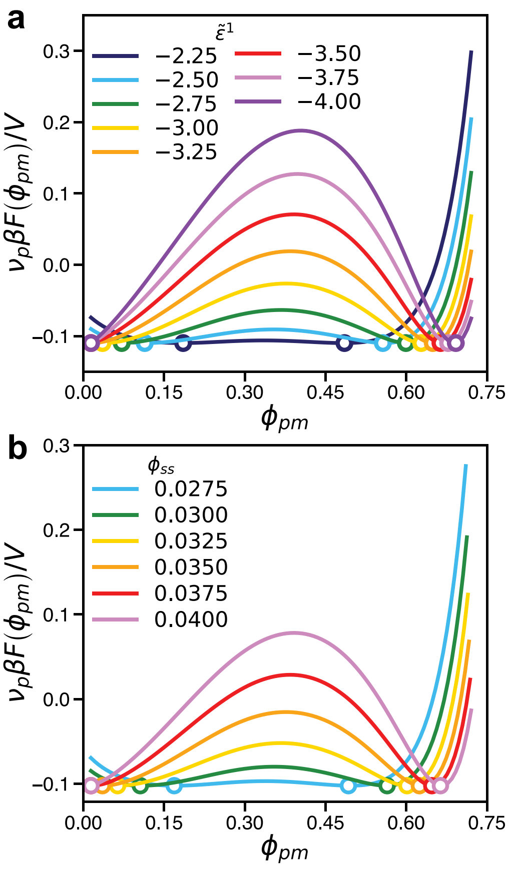

Figure 6. Plots of the free energy density $\nu_p \beta F/V$ vs polymer−micelle complex concentration ϕ_{pm} while varying (a) the correlation-based contribution to the polymer−micelle binding energy ε_m^1 and (b) the volume fraction of charged interacting surfactant headgroups contained within surface collocation point ϕ_{ss}. A linear shift factor of $a \times \phi_{pm}$ was added with prefactor a chosen such that the free energy values at the common tangent points (shown as open circles) are approximately equal.

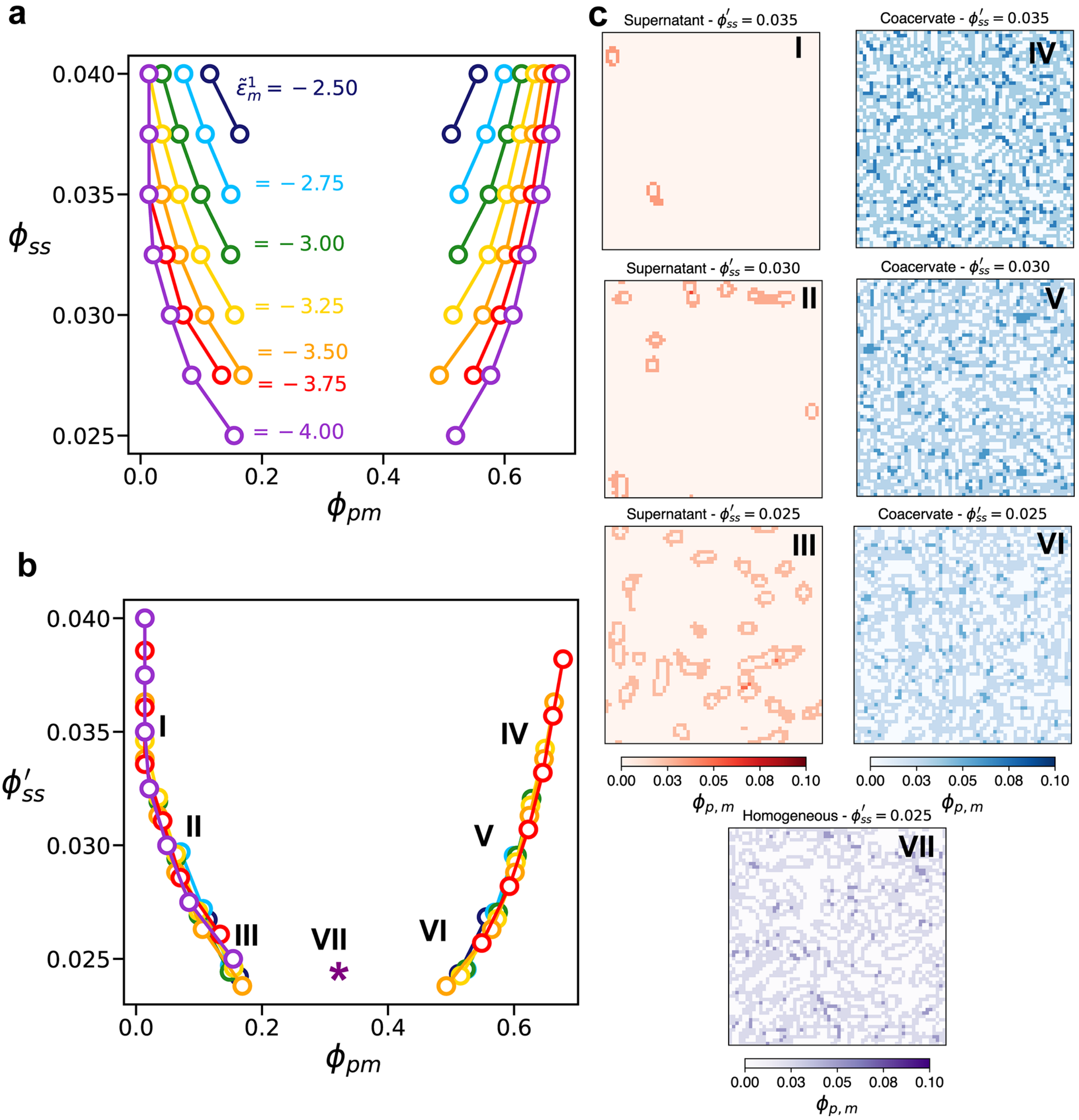

Figure 7. (a) Plot of surface charge density ϕ_{ss} as a function of the polymer−micelle complex concentration ϕ_{pm} in the supernatant (left series) and coacervate (right series) phases. Different colors correspond to different values of $\tilde{\varepsilon}_m^1$, with larger magnitudes corresponding to stronger polymer-mediated micelle−micelle attractions. (b) These curves can be shifted vertically by defining a new $\phi'_{ss} = \phi_{ss} - \Delta\phi_{ss}(\tilde{\varepsilon}_m^1)$, so that these phase boundaries collapse to a single universal curve. This collapse directly relates the surface charge density ϕ_{ss} to the electrostatic attraction between micelles $\tilde{\varepsilon}_m^1$. (c) Snapshots of the MC-informed grids for micelle-bound polymer density around the surfactant micelles, at values of ϕ_{pm} as indicated with corresponding Roman numerals in (b). Snapshots I−III are in the supernatant phase, snapshots IV−VI are in the coacervate phase, and snapshot VII is roughly at the concentration expected for the critical point. Colors are darker with more polyelectrolyte density, with especially dark colors located where two micelles come into close proximity.

systems. We expect this to be closely related to the length of the grafted PEG chains n, which exerts a steric repulsion that prevents the close approach of two neighboring micelles and thus weakens the strength of interaction that polyelectrolytes can have between two micelles simultaneously. Consistent with this physical picture, the value of $\phi_{pm}^c - \phi_{pm}^s$ decreased as the magnitude of $\tilde{\varepsilon}_m^1$ was decreased, such that increased steric repulsion weakens phase separation. When the magnitude of $|\tilde{\varepsilon}_m^1| < 2.25$, a critical point is approached as the coacervate and common tangent points meet and the coexistence region disappears.

Figure 6b shows the free energy curves for systems with $\tilde{\varepsilon}_m^1 = -3.5$ and varying values for ϕ_{ss} ranging from $\phi_{ss} = 0.0275$ to $\phi_{ss} = 0.04$. We consider that increasing the value of ϕ_{ss} in our theory corresponds to increasing the fraction of anionic surfactant *Y* in the experimental system. The specific correspondence between the theoretical and experimental values will be related to the volume of the charge surfactant headgroups contained within the surface collocation point as well as the corresponding volume of the adsorbing monomers (which are assumed to be equivalent on a per-charge basis). Because of this simplifying assumption, we do not attempt to make a quantitative matching but do expect a linear relationship between the fraction of anionic surfactant to ϕ_{ss}. Figure 6b demonstrates free energy landscapes labeled with the common tangent points, with all plotted landscapes showing phase separation. Consistent with experiments in the literature,[11,55] we observe that an increase in micellar surface charge density ϕ_{ss} leads to stronger phase separation due to the concomitant increase in electrostatic attractions between the micelles. Phase separation no longer occurs below $\phi_{ss} = 0.0275$ for this specific value of $\tilde{\varepsilon}_m^1$.

Figure 7a compiles the predictions from Figure 6 into a single plot for all combinations of ϕ_{ss} and $\tilde{\varepsilon}_m^1$, plotting the coexisting supernatant and coacervate concentrations ϕ_{pm}. Each different color corresponds to a different binding energy $\tilde{\varepsilon}_m^1$, which approaches miscibility such that the coexistence regime shrinks as the surface density of charged surfactant value ϕ_{ss} is lowered. Interestingly, this shrinking of the coexistence regime with ϕ_{ss} appears to be invariant to the choice of $\tilde{\varepsilon}_m^1$, except that it is shifted vertically with respect to ϕ_{ss}. We can show this more clearly by overlaying the various $\tilde{\varepsilon}_m^1$ curves, using a shift factor $\Delta\phi_{ss}$ such that we use a new *y*-axis $\phi'_{ss} = \phi_{ss} - \Delta\phi_{ss}(\tilde{\varepsilon}_m^1)$ in Figure 7b. Here we have defined the reference as $\Delta\phi_{ss}(\tilde{\varepsilon}_m^1 = -4.00) = 0$. With a judicious choice of the shift factors, we demonstrate that the coexistence curves collapse to a single universal curve; this means that in our model there is a direct correspondence between the surface charge density and the correlation-based interaction energy such that they have related effects on coacervation phase behavior. It is possible to observe the same phase separation behavior by simultaneously increasing the correlation interaction energy $\tilde{\varepsilon}_m^1$ and decreasing the fraction of charged surfactants ϕ_{ss}.

In Figure 7c we show representative snapshots of the micelle structures at the locations indicated in Figure 7b with Roman numerals. These are the density maps for the micelle-bound polyelectrolyte $\phi_{p,m}$, which outlines the surfaces of the micelles. The colors are especially dark at locations where micelles are in close proximity, leading to favorable polyelectrolyte interactions at these locations. For large values of ϕ'_{ss}, where the surface density of charges is large, there is a significant difference between the supernatant (I) and coacervate (IV) phases. The supernatant phase is extremely dilute, while the coacervate phase is almost completely packed with micelle structures. The disparity between these two phases decreases with ϕ'_{ss}, but there is always a marked structural difference between the coacervate and supernatant phases. There is a similarly large structural difference between both of these phases and the center of the coexistence regime (near the critical point, shown as VII).

Coacervate Phase Map of Surfactant Micelle Surface Charge versus Correlated Micelle–Micelle Attractions. In the previous sections, we demonstrated how we were able to obtain phase behavior from both experiment and our theory/simulation hybrid model, where the former was determined by turbidity measurements and the latter was determined from calculating the free energy of coacervate formation. We considered two sets of related quantities; for experiments these were the fraction of charged surfactant molecules Y and the PEG repeat unit n, while for the hybrid model they were the volume fraction of surface sites ϕ_{ss} and the strength of the charge correlation interaction $\tilde{\varepsilon}_m^1$. In general, we observed that coacervation was induced by increasing the fraction of charged surfactants Y (increasing ϕ_{ss}) or decreasing the length of the PEG grafted chains n (increasing $\tilde{\varepsilon}_m^1$). These values are not quantitatively equivalent, as this would require parametrizing (i) the value $\phi_{ss,0}$ of the volume fraction of surface sites for a fully charged surfactant micelle and (ii) the specific relationship between $\tilde{\varepsilon}_m^1$ and n^{-1}. This parametrization would require molecular simulation for this chemistry, which we do not pursue here, and instead focus on comparing physical trends rather than making quantitative predictions.

We can map out the phase behavior from both experiment and theory/simulation to show that these approaches give consistent results. In Figure 8a, we plot the critical charged surfactant molecule fraction Y_c as a function of the inverse PEG length n^{-1} for two different polyelectrolyte charge fractions. For the fully charged PTMAEMA, we show a nearly linear relationship between Y_c and n^{-1} over the entire range of PEG lengths tested, $n = 6$–23. We show a linear fit to this data as a phase boundary, above which phase separation occurs and below which the system is miscible. This is a manifestation of the trade-off between charge fraction and steric micelle–micelle repulsion seen in Figure 4 and corresponding to two molecular routes to tuning the surfactant–polyelectrolyte coacervate phase behavior.

The phase boundary shifts to larger values of Y_c for the 75% charge density PTMAEMA-*r*-HEMA copolymer due to the weaker electrostatic interactions from the polyelectrolyte (Figure 8a). A linear fit is again included on the plot to denote the approximate phase boundary, though the form of this boundary cannot be fully determined as only two points were measurable ($n = 6$ and $n = 7$). With this caveat, however, we note the slope of the phase boundary is steeper than in the fully charged case; this suggests a significant codependency on the polyelectrolyte charge density and its micelle induced correlation effects in driving phase separation.

In Figure 8b, we show the analogous phase diagram from our hybrid simulation/theory model. We show values of ϕ_{ss} and $-\tilde{\varepsilon}_m^1$ where our theory was evaluated as single-phase (open points) and two-phase (filled points). Similar to the experimental phase diagram, we observed a two-phase region at large surface charge density ϕ_{ss} and strong micelle–micelle correlation-based attractions $-\tilde{\varepsilon}_m^1$. A phase boundary was determined to correspond to the transition between the two regimes, but also so that it is consistent with the shift factor $\Delta\phi_{ss}(\tilde{\varepsilon}_m^1)$ calculated by collapsing the phase diagrams in Figure 7b. Similar to the experimental data, this phase boundary is roughly linear and again exhibits the same trade-off between micelle surface charge density and the polyelectrolyte-mediated, attractive interactions between micelles. This overall result agrees with the phenomenology seen in experiments, where phase separation occurs at high micelle surface charges and strong polyelectrolyte-driven micelle–micelle correlations. In the simulation/theory model we only considered a fully charged polyelectrolyte and note that polyelectrolyte charge sequence or fraction represents an interesting direction for future study.

■ CONCLUSION

We used a combination of experiment and modeling to understand how molecular interactions govern the phase behavior of polyelectrolyte–surfactant coacervates. Experimen-

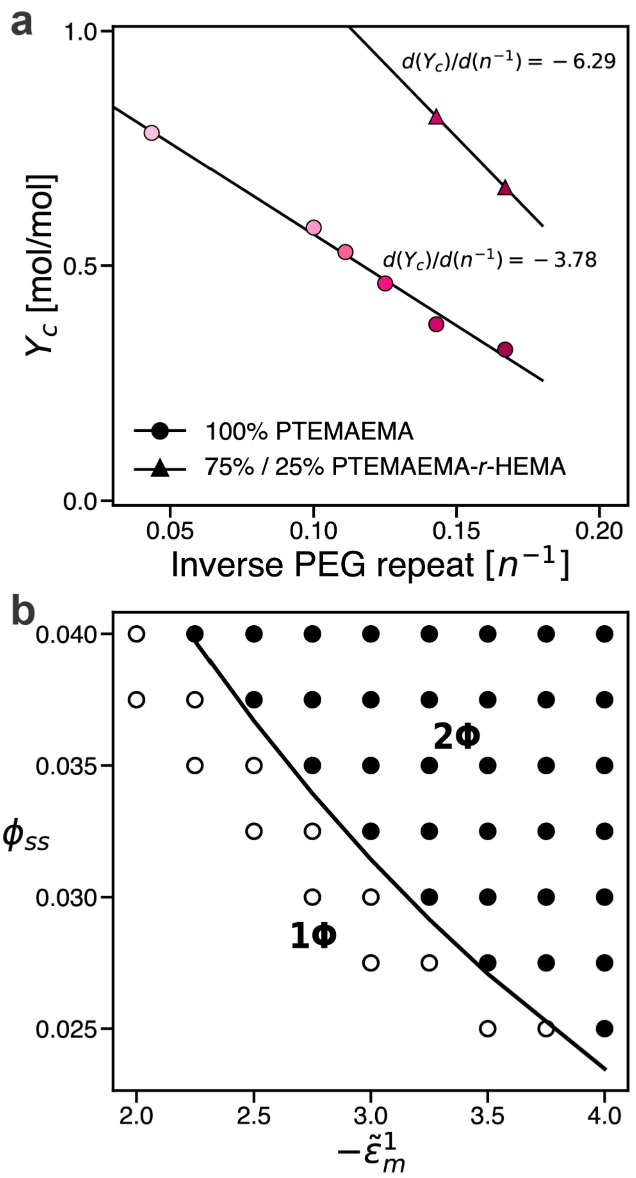

Figure 8. (a) Experimental phase diagram plotting the critical fraction of charged surfactants Y_c as a function of inverse PEG repeat length n^{-1} for complexes formed using the 100% charged PTMAEMA (circles) and the 75% charged PTMAEMA-*r*-HEMA (triangles). Fit lines represent approximate phase boundaries, such that polyelectrolyte–surfactant solutions with surfactant mixtures of $Y > Y_c$ (i.e., above the lines) will undergo coacervation. Slopes of fit lines are indicated on the graph and reflect the trade-off of electrostatic attraction vs steric repulsion in affecting the propensity of the system to undergo phase separation. (b) Phase diagram predicted by our hybrid simulation/theory model, where points denote the specific conditions considered in our calculations (defined by the surface-site volume fraction ϕ_{ss} and correlation-induced interaction energy $\tilde{\varepsilon}_m^1$). Each condition either underwent phase separation (filled points) or was miscible (open points), and we indicate an approximate phase boundary that is consistent with these observations as well as the shift factors determined from Figure 7b.

tally, the electrostatic interactions were varied by changing the fraction of charged surfactants Y in mixtures of ionic and neutral surfactants. Above a critical charged surfactant fraction $Y > Y_c$, coacervation was observed by both turbidity and microscopy measurements. Electrostatic interactions were also modulated by changing the charged fraction of the polyelectrolyte species, with coacervation being suppressed for polyelectrolytes with charge fractions <75% for the surfactant systems considered here. Short-ranged interactions were also tuned by including PEG chains of length n onto the neutral surfactants that can exert steric repulsions between nearby surfactant micelles. The value of Y_c decreased with decreasing n (increasing n^{-1}), such that coacervation occurred more readily when steric repulsions were weak.

We also used a simulation-informed field theory model to make predictions for coacervation in polyelectrolyte–surfactant solutions. Our model accounts for the thermodynamics of polyelectrolyte chains in the presence of external potential fields corresponding to the surfactant micelles, which are constructed from snapshots of coarse-grained MC simulations. Interactions between the polyelectrolyte and micelle surfaces were assumed to be strongly paired, and there is a volume fraction of surface sites ϕ_{ss} that is assumed to be proportional to Y_c. Strong, correlated electrostatics between micelles were accounted for by an interaction energy contribution $\tilde{\varepsilon}_m^1$ that quantifies the short-ranged micelle–micelle interactions and is related to the experimental quantity n. Coacervation was predicted by calculating the free energy $\nu_p \beta F/V$ as a function of the micelle surfactant concentration ϕ_{pm}. We observed phase separation at large values of ϕ_{ss} and $\tilde{\varepsilon}_m^1$ and demonstrated that there is a correspondence between these two parameters allowing us to collapse the phase diagrams onto a single curve defined by a shifted ϕ'_{ss}. Our predictions also allowed us to visualize the structure of the coacervate and supernatant phases and the spatial distribution of micelle and polyelectrolyte species.

The experimental and modeling results were compared by plotting both on a $Y_c(\phi_{ss})$ versus $n^{-1}(\tilde{\varepsilon}_m^1)$ phase diagram, with both cases exhibiting a similar phase boundary separating the two-phase and one-phase regime. The two-phase coacervate regime occurs at high micelle surface charge density and weak micelle–micelle repulsion (or strong micelle–micelle attraction), showing that both electrostatics and short-ranged interactions play a role in the phase behavior of surfactant–polyelectrolyte coacervates. This connects several molecular parameters (surfactant chemistry, mixtures, and polyelectrolyte charge fraction) to their corresponding bulk thermodynamics.

This favorable comparison between the experimental and modeling approaches establishes a basis for further probing the molecular interactions in these surfactant–polyelectrolyte systems. We envision further refinement of this model to address its current limitations. Important next steps would be to (i) determine the parameters such as $\tilde{\varepsilon}_m^1$ from more detailed models, (ii) account for different micelle geometries or morphologies (e.g., spherical, ordered phases), (iii) incorporate consistency between the MC and SCFT portions of the model so that micelle configuration can be affected by polyelectrolyte interactions, and (iv) account for polyelectrolyte charge fraction or sequence. These would connect with experimental observables (i.e., scattering) or parameters (e.g., surfactant chemistry and polymer sequence) that will allow us to refine our physical understanding of surfactant–polyelectrolyte systems. In addition, both experiment and modeling would be considered over a more extensive parameter space, capturing the competition and partitioning of the five (or more) components in these systems as they undergo phase separation.

■ ASSOCIATED CONTENT

Supporting Information

The Supporting Information is available free of charge at https://pubs.acs.org/doi/10.1021/acs.macromol.3c00464.

> ^{1}H NMR spectra for TMAEMA monomer, RAFT copolymerization scheme, table describing the characterization of synthesized copolyelectrolytes, ^{1}H NMR spectra analysis of copolymer composition, and indication of ^{1}H NMR peak used for DOSY analysis (PDF)

■ AUTHOR INFORMATION

Corresponding Authors

Charles E. Sing − *Department of Chemical & Biomolecular Engineering, University of Illinois at Urbana−Champaign, Urbana, Illinois 61801, United States;* orcid.org/0000-0001-7231-2685; Email: cesing@illinois.edu

Sarah L. Perry − *Department of Chemical Engineering, University of Massachusetts Amherst, Amherst, Massachusetts 01003, United States;* orcid.org/0000-0003-2301-6710; Email: perrys@engin.umass.edu

Authors

Jason J. Madinya − *Department of Chemical & Biomolecular Engineering, University of Illinois at Urbana−Champaign, Urbana, Illinois 61801, United States;* orcid.org/0000-0002-1401-8098

Hansen Tjo − *Department of Chemical Engineering, University of Massachusetts Amherst, Amherst, Massachusetts 01003, United States*

Xiangxi Meng − *Department of Chemical Engineering, University of Massachusetts Amherst, Amherst, Massachusetts 01003, United States;* orcid.org/0000-0003-3886-7892

Isaac A. Ramírez Marrero − *Department of Chemical Engineering, University of Massachusetts Amherst, Amherst, Massachusetts 01003, United States;* orcid.org/0000-0003-0519-6017

Complete contact information is available at:
https://pubs.acs.org/10.1021/acs.macromol.3c00464

Notes

The authors declare no competing financial interest.

■ ACKNOWLEDGMENTS

J.J.M. acknowledges support by the National Science Foundation Graduate Research Fellowship Program under Grant DGE-1746047 and the Sloan Minority PhD Program. C.E.S. and J.J.M. acknowledge support by the National Science Foundation under Grant DMR-1654158. H.T. acknowledges support by the University of Massachusetts Amherst Commonwealth Honors College. X.M. and S.L.P. acknowledge support from the National Science Foundation under Grant CMMI-1727660. I.R.M. and S.L.P. acknowledge support from BASF. We thank Dr. Weiguo Hu for assistance with DOSY experiments and providing the PMMA molecular weight correlation function. Nuclear magnetic resonance data were obtained at the University of Massachusetts NMR Core Facility. We also thank Rainer Gutzler, Rupert Konradi, and Bernhard von Vacano for the PTMAEMA homopolymer. We also thank Mingjun Zhou for helpful discussions and the late Paul Dubin for his early mentoring support on this project.

■ REFERENCES

(1) Dubin, P. L.; Curran, M. E.; Hua, J. Critical Linear Charge Density for Binding of a Weak Polycation to an Anionic/Nonionic Mixed Micelle. *Langmuir* **1990**, *6*, 707−709.

(2) Wang, Y.; Kimura, K.; Huang, Q.; Dubin, P. L.; Jaeger, W. Effects of Salt on Polyelectrolyte-Micelle Coacervation. *Macromolecules* **1999**, *32*, 7128−7134.

(3) Wang, Y.; Kimura, K.; Dubin, P. L.; Jaeger, W. Polyelectrolyte-Micelle Coacervation: Effects of Micelle Surface Charge Density, Polymer Molecular Weight, and Polymer/Surfactant Ratio. *Macromolecules* **2000**, *33*, 3324−3331.

(4) Kizilay, E.; Kayitmazer, A. B.; Dubin, P. L. Complexation and Coacervation of Polyelectrolytes with Oppositely Charged Colloids. *Adv. Colloid Interface Sci.* **2011**, *167*, 24−37.

(5) Gradzielski, M.; Hoffmann, I. Polyelectrolyte-Surfactant Complexes (PESCs) Composed of Oppositely Charged Components. *Curr. Opin. Colloid Interface Sci.* **2018**, *35*, 124−141.

(6) Thalberg, K.; Lindman, B.; Karlstroem, G. Phase Behavior of Systems of Cationic Surfactant and Anionic Polyelectrolyte: Influence of Surfactant Chain Length and Polyelectrolyte Molecular Weight. *J. Phys. Chem.* **1991**, *95*, 3370−3376.

(7) Zhao, W.; Wang, Y. Coacervation with Surfactants: From Single-Chain Surfactants to Gemini Surfactants. *Adv. Colloid Interface Sci.* **2017**, *239*, 199−212.

(8) Liberatore, M. W.; Wyatt, N. B.; Henry, M.; Dubin, P. L.; Foun, E. Shear-Induced Phase Separation in Polyelectrolyte/Mixed Micelle Coacervates. *Langmuir* **2009**, *25*, 13376−13383.

(9) Zhao, M.; Wang, C.; Jiang, H.; Dawadi, M. B.; Vogt, B. D.; Modarelli, D. A.; Zacharia, N. S. Polyelectrolyte-Micelle Coacervates: Intrapolymer-Dominant vs. Interpolymer-Dominant Association, Solute Uptake and Rheological Properties. *Soft Matter* **2019**, *15*, 3043−3054.

(10) Thalberg, K.; Lindman, B.; Bergfeldt, K. Phase Behavior of Systems of Polyacrylate and Cationic Surfactants. *Langmuir* **1991**, *7*, 2893−2898.

(11) McQuigg, D. W.; Kaplan, J. I.; Dubin, P. L. Critical Conditions for the Binding of Polyelectrolytes to Small Oppositely Charged Micelles. *J. Phys. Chem.* **1992**, *96*, 1973−1978.

(12) Chronakis, I. S.; Alexandridis, P. Rheological Properties of Oppositely Charged Polyelectrolyte- Surfactant Mixtures: Effect of Polymer Molecular Weight and Surfactant Architecture. *Macromolecules* **2001**, *34*, 5005−5018.

(13) Li, Y.; Xia, J.; Dubin, P. L. Complex Formation between Polyelectrolyte and Oppositely Charged Mixed Micelles: Static and Dynamic Light Scattering Study of the Effect of Polyelectrolyte Molecular Weight and Concentration. *Macromolecules* **1994**, *27*, 7049−7055.

(14) Li, Y.; Dubin, P. L.; Dautzenberg, H.; Lueck, U.; Hartmann, J.; Tuzar, Z. Dependence of Structure of Polyelectrolyte/Micelle Complexes upon Polyelectrolyte Chain Length and Micelle Size. *Macromolecules* **1995**, *28*, 6795−6798.

(15) Seyrig, C.; Le Griel, P.; Cowieson, N.; Perez, J.; Baccile, N. Synthesis of Multilamellar Walls Vesicles Polyelectrolyte-Surfactant Complexes from pH-Stimulated Phase Transition Using Microbial Biosurfactants. *J. Colloid Interface Sci.* **2020**, *580*, 493−502.

(16) Marciel, A. B.; Srivastava, S.; Tirrell, M. V. Structure and rheology of polyelectrolyte complex coacervates. *Soft Matter* **2018**, *14*, 2454−2464.

(17) Liu, Y.; Santa Chalarca, C.; Carmean, R.; Olson, R.; Madinya, J.; Sumerlin, B.; Sing, C.; Emrick, T.; Perry, S. Effect of Polymer Chemistry on the Linear Viscoelasticity of Complex Coacervates. *Macromolecules* **2020**, *53*, 7851−7864.

(18) Priftis, D.; Xia, X.; Margossian, K. O.; Perry, S. L.; Leon, L.; Qin, J.; de Pablo, J. J.; Tirrell, M. Ternary, Tunable Polyelectrolyte Complex Fluids Driven by Complex Coacervation. *Macromolecules* **2014**, *47*, 3076−3085.

(19) Spruijt, E.; Sprakel, J.; Lemmers, M.; Stuart, M. A. C.; van der Gucht, J. Relaxation Dynamics at Different Time Scales in

Electrostatic Complexes: Time-Salt Superposition. *Phys. Rev. Lett.* **2010**, *105*, 208301.

(20) Larson, R. G.; Liu, Y.; Li, H. Linear Viscoelasticity and Time-Temperature-Salt and Other Superpositions in Polyelectrolyte Coacervates. *J. Rheol.* **2021**, *65*, 77−102.

(21) Liu, Y.; Momani, B.; Winter, H. H.; Perry, S. L. Rheological Characterization of Liquid-to-Solid Transitions in Bulk Polyelectrolyte Complexes. *Soft Matter* **2017**, *13*, 7332−7340.

(22) Liu, Y.; Winter, H. H.; Perry, S. L. Linear Viscoelasticity of Complex Coacervates. *Adv. Colloid Interface Sci.* **2017**, *239*, 46−60.

(23) Dubin, P. L.; Li, Y.; Jaeger, W. Mesophase Separation in Polyelectrolyte-Mixed Micelle Coacervates. *Langmuir* **2008**, *24*, 4544−4549.

(24) Radhakrishna, M.; Basu, K.; Liu, Y.; Shamsi, R.; Perry, S. L.; Sing, C. E. Molecular Connectivity and Correlation Effects on Polymer Coacervation. *Macromolecules* **2017**, *50*, 3030−3037.

(25) Blocher McTigue, W. C.; Perry, S. L. Design Rules for Encapsulating Proteins into Complex Coacervates. *Soft Matter* **2019**, *15*, 3089−3103.

(26) Zhang, P.; Shen, K.; Alsaifi, N. M.; Wang, Z.-G. Salt partitioning in complex coacervation of symmetric polyelectrolytes. *Macromolecules* **2018**, *51*, 5586−5593.

(27) Zhao, W.; Fan, Y.; Wang, H.; Wang, Y. Coacervate of Polyacrylamide and Cationic Gemini Surfactant for the Extraction of Methyl Orange from Aqueous Solution. *Langmuir* **2017**, *33*, 6846−6856.

(28) Schmitt, C.; Turgeon, S. L. Protein/Polysaccharide Complexes and Coacervates in Food Systems. *Adv. Colloid Interface Sci.* **2011**, *167*, 63−70.

(29) Sharipova, A.; Aidarova, S.; Grigoriev, D.; Mutalieva, B.; Madibekova, G.; Tleuova, A.; Miller, R. Polymer-Surfactant Complexes for Microencapsulation of Vitamin E and its Release. *Colloids Surf., B* **2016**, *137*, 152−157.

(30) Laquerbe, S.; Carvalho, A.; Schmutz, M.; Poirier, A.; Baccile, N.; Messaoud, G. B. pH-Switchable Pickering Emulsions Stabilized by Polyelectrolyte-Biosurfactant Complex Coacervate Colloids. *J. Colloid Interface Sci.* **2021**, *600*, 23−36.

(31) Benhur, A. M.; Diaz, J.; Amin, S. Impact of Polyelectrolyte-Surfactant Interactions on the Rheology and Wet Lubrication Performance of Conditioning Shampoo. Int. *J. Cosmet. Sci.* **2021**, *43*, 246−253.

(32) Hiwatari, Y.; Yoshida, K.; Akutsu, T.; Yabu, M.; Iwai, S. Polyelectrolyte-Micelle Coacervation: Effect of Coacervate on the Properties of Shampoo. Int. *J. Cosmet. Sci.* **2004**, *26*, 316−316.

(33) Llamas, S.; Guzman, E.; Ortega, F.; Baghdadli, N.; Cazeneuve, C.; Rubio, R. G.; Luengo, G. S. Adsorption of Polyelectrolytes and Polyelectrolytes-Surfactant Mixtures at Surfaces: A Physico-chemical Approach to a Cosmetic Challenge. *Adv. Colloid Interface Sci.* **2015**, *222*, 461−487.

(34) Kristen, N.; von Klitzing, R. Effect of Polyelectrolyte/Surfactant Combinations on the Stability of Foam Films. *Soft Matter* **2010**, *6*, 849−861.

(35) Kalantar, T. H.; Tucker, C. J.; Zalusky, A. S.; Boomgaard, T. A.; Wilson, B. E.; Ladika, M.; Jordan, S. L.; Li, W. K.; Xhang, X. High Throuhgput Workflow for Coacervate Formation and Characterization in Shampoo Systems. *J. Cosmet. Sci.* **2007**, *58*, 375−383.

(36) Mayya, K. S.; Bhattacharyya, A.; Argillier, J.-F. Microencapsulation by Complex Coacervation: Influence of Surfactant. *Polym. Int.* **2003**, *52*, 644−647.

(37) Mirtič, J.; Kogej, K.; Baumgartner, S.; Smistad, G.; Kristl, J.; Hiorth, M. Development of Cetylpyridinium-Alginate Nanoparticles: A Binding and Formulation Study. *Int. J. Pharm.* **2016**, *511*, 774−784.

(38) de Silva, U. K.; Brown, J. L.; Lapitsky, Y. Poly(allylamine)/Tripolyphosphate Coacervates Enable High Loading and Multiple-month Release of Weakly Amphiphilic Anionic Drugs: An in vitro Study with Ibuprofen. *RSC Adv.* **2018**, *8*, 19409−19419.

(39) Jain, N.; Trabelsi, S.; Guillot, S.; McLoughlin, D.; Langevin, D.; Letellier, P.; Turmine, M. Critical Aggregation Concentration in Mixed solutions of Anionic Polyelectrolytes and Cationic Surfactants. *Langmuir* **2004**, *20*, 8496−8503.

(40) Kogej, K.; Škerjanc, J. Fluorescence and Conductivity Studies of Polyelectrolyte-Induced Aggregation of Alkyltrimethylammonium Bromides. *Langmuir* **1999**, *15*, 4251−4258.

(41) Berret, J.-F. Controlling Electrostatic Co-assembly Using Ion-containing Copolymers: From Surfactants to Nanoparticles. *Adv. Colloid Interface Sci.* **2011**, *167*, 38−48.

(42) Guzmán, E.; Fernández-Peña, L.; Ortega, F.; Rubio, R. G. Equilibrium and Kinetically Trapped Aggregates in Polyelectrolyte-Oppositely Charged Surfactant Mixtures. *Curr. Opin. Colloid Interface Sci.* **2020**, *48*, 91−108.

(43) Guillot, S.; McLoughlin, D.; Jain, N.; Delsanti, M.; Langevin, D. Polyelectrolyte-Surfactant Complexes at Interfaces and in Bulk. *J. Phys.: Condens. Matter* **2003**, *15*, S219.

(44) Wallin, T.; Linse, P. Polyelectrolyte-Induced Micellization of Charged Surfactants. Calculations Based on a Self-Consistent Field Lattice Model. *Langmuir* **1998**, *14*, 2940−2949.

(45) Bodnár, K.; Fegyver, E.; Nagy, M.; Mészáros, R. Impact of Polyelectrolyte Chemistry on the Thermodynamic Stability of Oppositely Charged Macromolecule/Surfactant Mixtures. *Langmuir* **2016**, *32*, 1259−1268.

(46) Lam, V. D.; Walker, L. M. A pH-induced Transition of Surfactant-Polyelectrolyte Aggregates from Cylindrical to String-of-Pearls Structure. *Langmuir* **2010**, *26*, 10489−10496.

(47) Goswami, M.; Borreguero, J. M.; Pincus, P. A.; Sumpter, B. G. Surfactant-Mediated Polyelectrolyte Self-Assembly in a Polyelectrolyte-Surfactant Complex. *Macromolecules* **2015**, *48*, 9050−9059.

(48) Chiappisi, L.; Hoffmann, I.; Gradzielski, M. Complexes of Oppositely Charged Polyelectrolytes and Surfactants - Recent Developments in the Field of Biologically Derived Polyelectrolytes. *Soft Matter* **2013**, *9*, 3896−3909.

(49) Piculell, L. Understanding and Exploiting the Phase Behavior of Mixtures of Oppositely Charged Polymers and Surfactants in Water. *Langmuir* **2013**, *29*, 10313−10329.

(50) Li, Y.; Dubin, P. L.; Havel, H. A.; Edwards, S. L.; Dautzenberg, H. Complex Formation Between Polyelectrolyte and Oppositely Charged Mixed Micelles: Soluble Complexes vs Coacervation. *Langmuir* **1995**, *11*, 2486−2492.

(51) Li, D.; Kelkar, M. S.; Wagner, N. J. Phase Behavior and Molecular Thermodynamics of Coacervation in Oppositely Charged Polyelectrolyte/Surfactant Systems: A Cationic Polymer JR 400 and Anionic Surfactant SDS Mixture. *Langmuir* **2012**, *28*, 10348−10362.

(52) Messaoud, G. B.; Promeneur, L.; Brennich, M.; Roelants, S. L.; Le Griel, P.; Baccile, N. Complex Coacervation of Natural Sophorolipid Bolaamphiphile Micelles with Cationic Polyelectrolytes. *Green Chem.* **2018**, *20*, 3371−3385.

(53) Guillemet, F.; Piculell, L. Interactions in Aqueous Mixtures of Hydrophobically Modified Polyelectrolyte and Oppositely Charged Surfactant. Mixed Micelle Formation and Associative Phase Separation. *J. Phys. Chem.* **1995**, *99*, 9201−9209.

(54) Svensson, A.; Piculell, L.; Cabane, B.; Ilekti, P. A New Approach to the Phase Behavior of Oppositely Charged Polymers and Surfactants. *J. Phys. Chem. B* **2002**, *106*, 1013−1018.

(55) Fan, Y.; Kellermeier, M.; Xu, A. Y.; Boyko, V.; Mirtschin, S.; Dubin, P. L. Modulation of Polyelectrolyte-Micelle Interactions via Zeta Potentials. *Macromolecules* **2017**, *50*, 5518−5526.

(56) Dubin, P. L.; Oteri, R. Association of Polyelectrolytes with Oppositely Charged Mixed Micelles. *J. Colloid Interface Sci.* **1983**, *95*, 453−461.

(57) Dubin, P. L.; Davis, D. Stoichiometry and Coacervation of Complexes Formed Between Polyelectrolytes and Mixed Micelles. *Colloids Surf.* **1985**, *13*, 113−124.

(58) Comert, F.; Nguyen, D.; Rushanan, M.; Milas, P.; Xu, A. Y.; Dubin, P. L. Precipitate-Coacervate Transformation in Polyelectrolyte-Mixed Micelle Systems. *J. Phys. Chem. B* **2017**, *121*, 4466−4473.

(59) Cooper, C. L.; Goulding, A.; Kayitmazer, A. B.; Ulrich, S.; Stoll, S.; Turksen, S.; Yusa, S.-i.; Kumar, A.; Dubin, P. L. Effects of Polyelectrolyte Chain Stiffness, Charge Mobility, and Charge

Sequences on Binding to Proteins and Micelles. *Biomacromolecules* **2006**, *7*, 1025−1035.

(60) Zhang, H.; Li, Y.; Dubin, P.; Kato, T. Effect of EO Chain Length of Dodecanol Ethoxylates ($C_{12}E_n$) on the Complexation of $C_{12}E_n$/SDS Mixed Micelles with an Oppositely Charged Polyelectrolyte. *J. Colloid Interface Sci.* **1996**, *183*, 546−551.

(61) Fegyver, E.; Mészáros, R. The Impact of Nonionic Surfactant Additives on the Nonequilibrium Association Between Oppositely Charged Polyelectrolytes and Ionic Surfactants. *Soft Matter* **2014**, *10*, 1953−1962.

(62) Israelachvili, J. N.; Mitchell, D. J.; Ninham, B. W. Theory of Self-Assembly of Hydrocarbon Amphiphiles into Micelles and Bilayers. *J. Chem. Soc., Faraday Trans. 2* **1976**, *72*, 1525−1568.

(63) Taylor, D.; Thomas, R.; Penfold, J. Polymer/Surfactant Interactions at the Air/Water Interface. *Adv. Colloid Interface Sci.* **2007**, *132*, 69−110.

(64) Janiak, J.; Piculell, L.; Olofsson, G.; Schillén, K. The Aqueous Phase Behavior of Polyion-Surfactant Ion Complex Salts Mixed with Nonionic Surfactants. *Phys. Chem. Chem. Phys.* **2011**, *13*, 3126−3138.

(65) Fegyver, E.; Mészáros, R. Fine-Tuning the Nonequilibrium Behavior of Oppositely Charged Macromolecule/Surfactant Mixtures via the Addition of Nonionic Amphiphiles. *Langmuir* **2014**, *30*, 15114−15126.

(66) Tam, K. C.; Wyn-Jones, E. Insights on Polymer Surfactant Complex Structures During the Binding of Surfactants to Polymers as Measured by Equilibrium and Structural Techniques. *Chem. Soc. Rev.* **2006**, *35*, 693−709.

(67) Khan, N.; Brettmann, B. Intermolecular Interactions in Polyelectrolyte and Surfactant Complexes in Solution. *Polymers* **2019**, *11*, 51.

(68) Thalberg, K.; Lindman, B.; Karlstroem, G. Phase Diagram of a System of Cationic Surfactant and Anionic Polyelectrolyte: Tetradecyltrimethylammonium Bromide-Hyaluronan-Water. *J. Phys. Chem.* **1990**, *94*, 4289−4295.

(69) Li, D.; Wagner, N. J. Universal Binding Behavior for Ionic Alkyl Surfactants with Oppositely Charged Polyelectrolytes. *J. Am. Chem. Soc.* **2013**, *135*, 17547−17555.

(70) Satake, I.; Yang, J. T. Interaction of Sodium Decyl Sulfate with Poly(L-Ornithine) and Poly(L-Lysine) in Aqueous Solution. *Biopolymers* **1976**, *15*, 2263−2275.

(71) Lytle, T. K.; Sing, C. E. Transfer Matrix Theory of Polymer Complex Coacervation. *Soft Matter* **2017**, *13*, 7001−7012.

(72) Lytle, T. K.; Sing, C. E. Tuning Chain Interaction Entropy in Complex Coacervation using Polymer Stiffness, Architecture, and Salt Valency. *Mol. Syst. Des. Eng.* **2018**, *3*, 183−196.

(73) Lytle, T. K.; Salazar, A. J.; Sing, C. E. Interfacial Properties of Polymeric Complex Coacervates from Simulation and Theory. *J. Chem. Phys.* **2018**, *149*, 163315.

(74) Knoerdel, A. R.; Blocher McTigue, W. C.; Sing, C. E. Transfer Matrix Model of pH Effects in Polymeric Complex Coacervation. *J. Phys. Chem. B* **2021**, *125*, 8965−8980.

(75) Madinya, J. J.; Chang, L.-W.; Perry, S. L.; Sing, C. E. Sequence-Dependent Self-Coacervation in High Charge-Density Polyampholytes. *Mol. Syst. Des. Eng.* **2020**, *5*, 632−644.

(76) Borreguero, J. M.; Pincus, P. A.; Sumpter, B. G.; Goswami, M. Unraveling the Agglomeration Mechanism in Charged Block Copolymer and Surfactant Complexes. *Macromolecules* **2017**, *50*, 1193−1205.

(77) Wallin, T.; Linse, P. Monte Carlo Simulations of Polyelectrolytes at Charged Micelles. 2. Effects of Linear Charge Density. *J. Phys. Chem.* **1996**, *100*, 17873−17880.

(78) Wallin, T.; Linse, P. Monte Carlo Simulations of Polyelectrolytes at Charged Micelles. 3. Effects of Surfactant Tail Length. *J. Phys. Chem. B* **1997**, *101*, 5506−5513.

(79) Berret, J.-F.; Hervé, P.; Aguerre-Chariol, O.; Oberdisse, J. Colloidal Complexes Obtained from Charged Block Copolymers and Surfactants: A Comparison between Small-Angle Neutron Scattering, Cryo-TEM, and Simulations. *J. Phys. Chem. B* **2003**, *107*, 8111−8118.

(80) Groot, R. D. Electrostatic Interactions in Dissipative Particle Dynamics - Simulation of Polyelectrolytes and Anionic Surfactants. *J. Chem. Phys.* **2003**, *118*, 11265−11277.

(81) Wallin, T.; Linse, P. Monte Carlo Simulations of Polyelectrolytes at Charged Micelles. 1. Effects of Chain Flexibility. *Langmuir* **1996**, *12*, 305−314.

(82) Pryamitsyn, V.; Ganesan, V. Interplay Between Depletion and Electrostatic Interactions in Polyelectrolyte-Nanoparticle Systems. *Macromolecules* **2014**, *47*, 6095−6112.

(83) Pandav, G.; Pryamitsyn, V.; Errington, J.; Ganesan, V. Multibody Interactions, Phase Behavior, and Clustering in Nanoparticle-Polyelectrolyte Mixtures. *J. Phys. Chem. B* **2015**, *119*, 14536−14550.

(84) Samanta, R.; Ganesan, V. Direct Simulations of Phase Behavior of Mixtures of Oppositely Charged Proteins/Nanoparticles and Polyelectrolytes. *J. Phys. Chem. B* **2020**, *124*, 10943−10951.

(85) Samanta, R.; Halabe, A.; Ganesan, V. Influence of Charge Regulation and Charge Heterogeneity on Complexation Between Polyelectrolytes and Proteins. *J. Phys. Chem. B* **2020**, *124*, 4421−4435.

(86) Samanta, R.; Ganesan, V. Influence of Protein Charge Patches on the Structure of Protein-Polyelectrolyte Complexes. *Soft Matter* **2018**, *14*, 9475−9488.

(87) Rumyantsev, A. M.; Borisov, O. V.; de Pablo, J. J. Structure and Dynamics of Hybrid Colloid-Polyelectrolyte Coacervates. *Macromolecules* **2023**, *56* (4), 1713.

(88) Madinya, J. J.; Sing, C. E. Hybrid Field Theory and Particle Simulation Model of Polyelectrolyte-Surfactant Coacervation. *Macromolecules* **2022**, *55*, 2358−2373.

(89) Lytle, T. K.; Chang, L.-W.; Markiewicz, N.; Perry, S. L.; Sing, C. E. Designing Electrostatic Interactions via Polyelectrolyte Monomer Sequence. *ACS central science* **2019**, *5*, 709−718.

(90) Chang, L.-W.; Lytle, T. K.; Radhakrishna, M.; Madinya, J. J.; Vélez, J.; Sing, C. E.; Perry, S. L. Sequence and entropy-based control of complex coacervates. *Nat. Commun.* **2017**, *8*, 1−8.

(91) Perrier, S. 50th Anniversary Perspective: RAFT Polymerization A User Guide. *Macromolecules* **2017**, *50*, 7433−7447.

(92) Konkolewicz, D.; Siauw, M.; Gray-Weale, A.; Hawkett, B. S.; Perrier, S. Obtaining Kinetic Information from the Chain-Length Distribution of Polymers Produced by RAFT. *J. Phys. Chem. B* **2009**, *113*, 7086−7094.

(93) Siauw, M.; Hawkett, B. S.; Perrier, S. Short Chain Amphiphilic Diblock Co-Oligomers via RAFT Polymerization. *J. Polym. Sci., Part A: Polym. Chem.* **2012**, *50*, 187−198.

(94) Ferreira, G. A.; Loh, W. Liquid crystalline nanoparticles formed by oppositely charged surfactant-polyelectrolyte complexes. Current Opinion in Colloid. *Interface Science* **2017**, *32*, 11−22.

(95) Rharbi, Y.; Chen, L.; Winnik, M. A. Exchange Mechanisms for Sodium Dodecyl Sulfate Micelles: High Salt Concentration. *J. Am. Chem. Soc.* **2004**, *126*, 6025−6034.

(96) Yada, S.; Suzuki, T.; Hashimoto, S.; Yoshimura, T. Adsorption and Aggregation Properties of Homogeneous Polyoxypropylene-Polyoxyethylene Alkyl Ether Type Nonionic Surfactants. *Langmuir* **2017**, *33*, 3794−3801.

(97) Svensson, A.; Norrman, J.; Piculell, L. Phase Behavior of Polyion-Surfactant Ion Complex Salts: Effects of Surfactant Chain Length and Polyion Length. *J. Phys. Chem. B* **2006**, *110*, 10332−10340.

(98) Lauw, Y.; Leermakers, F. A. M.; Cohen Stuart, M. Persistence Length of Wormlike Micelles Composed of Ionic Surfactants: Self-Consistent-Field Predictions. *J. Phys. Chem. B* **2007**, *111*, 8158−8168.

(99) Solis, F. J.; de la Cruz, M. O. Collapse of flexible polyelectrolytes in multivalent salt solutions. *J. Chem. Phys.* **2000**, *112*, 2030−2035.

(100) Wang, Z.; Rubinstein, M. Regimes of conformational transitions of a diblock polyampholyte. *Macromolecules* **2006**, *39*, 5897−5912.

(101) Sing, C. E.; Qin, J. Bridging Field Theory and Ion Pairing in the Theory of Polymer Complex Coacervation. *ChemRxiv* 2023. DOI: DOI: 10.26434/chemrxiv-2023-v6x4f.

(102) Wong, G. C.; Pollack, L. Electrostatics of Strongly Charged Biological Polymers: Ion-Mediated Interactions and Self-Organization in Nucleic Acids and Proteins. *Annu. Rev. Phys. Chem.* **2010**, *61*, 171−189.

(103) Lau, A. W. C.; Lukatsky, D. B.; Pincus, P.; Safran, S. A. Charge fluctuations and counterion condensation. *Phys. Rev. E* **2002**, *65*, 051502.

(104) Moreira, A. G.; Netz, R. R. Binding of similarly charged plates with counterions only. *Physical review letters* **2001**, *87*, 078301.

(105) Netz, R. R. Electrostatistics of counter-ions at and between planar charged walls: From Poisson-Boltzmann to the strong-coupling theory. *Eur. Phys. J. E* **2001**, *5*, 557−574.

(106) Dahlgren, M. A. G.; Waltermo, A.; Blomberg, E.; Claesson, P. M.; Sjoestroem, L.; Aakesson, T.; Joensson, B. Salt effects on the interaction between adsorbed cationic polyelectrolyte layers: theory and experiment. *J. Phys. Chem.* **1993**, *97*, 11769−11775.

(107) Borukhov, I.; Andelman, D.; Orland, H. Effect of Polyelectrolyte Adsorption on Intercolloidal Forces. *J. Phys. Chem. B* **1999**, *103*, 5042−5057.

(108) Åkesson, T.; Woodward, C.; Jönsson, B. Electric double layer forces in the presence of polyelectrolytes. *J. Chem. Phys.* **1989**, *91*, 2461−2469.

(109) Fredrickson, G. *The Equilibrium Theory of Inhomogeneous Polymers*; Oxford University Press: 2006; Vol. *134*.

(110) Wang, Q.; Taniguchi, T.; Fredrickson, G. H. Self-Consistent Field Theory of Polyelectrolyte Systems. *J. Phys. Chem. B* **2004**, *108*, 6733−6744.

(111) Spruijt, E.; Leermakers, F. A. M.; Fokkink, R.; Schweins, R.; van Well, A. A.; Cohen Stuart, M. A.; van der Gucht, J. Structure and Dynamics of Polyelectrolyte Complex Coacervates Studied by Scattering of Neutrons, X-rays, and Light. *Macromolecules* **2013**, *46*, 4596−4605.

(112) Carnahan, N. F.; Starling, K. E. Equation of State for Nonattracting Rigid Spheres. *J. Chem. Phys.* **1969**, *51*, 635−636.

(113) Neitzel, A. E.; Fang, Y. N.; Yu, B.; Rumyantsev, A. M.; de Pablo, J. J.; Tirrell, M. V. Polyelectrolyte Complex Coacervation Across a Broad Range of Charge Densities. *Macromolecules* **2021**, *54*, 6878−6890.